DETECTING AND MODELING CEMENT FAILURE IN HIGH PRESSURE/HIGH TEMPERATURE WELLS, USING FINITE-ELEMENT METHOD

A Thesis

by

MEHDI ABBASZADEH SHAHRI

Submitted to the Office of the Graduate Studies of
Texas A&M University
in partial fulfillment of the requirements for the degree of

MASTER OF SCIENCE

December 2005

Major Subject: Petroleum Engineering

DETECTING AND MODELING CEMENT FAILURE IN HIGH PRESSURE/HIGH TEMPERATURE WELLS, USING FINITE-ELEMENT METHOD

A Thesis

by

MEHDI ABBASZADEH SHAHRI

Submitted to the Office of Graduate Studies of
Texas A&M University
in partial fulfillment of the requirements for the degree of

MASTER OF SCIENCE

Approved By:

Chair of Committee,	Jerome J. Schubert
Committee Members,	Hans C. Juvkam-Wold
	Reza Langari
Head of Department,	Stephen A. Holditch

December 2005

Major Subject: Petroleum Engineering

ABSTRACT

Detecting and Modeling Cement Failure in High Pressure/High Temperature Wells Using Finite-Element Method. (December 2005)

Mehdi Abbaszadeh Shahri, B.S., Petroleum University of Technology, Iran

Chair of Advisory Committee: Dr. Jerome. J. Schubert

A successful cement job results in complete zonal isolation while saving time and money. To achieve these goals, various factors such as well security, casing centralization, effective mud removal, and gas migration must be considered in the design. In the event that high-pressure and high-temperature (HPHT) conditions are encountered, we must attempt to achieve permeability in the set cement to prevent gas migration and to prevent any other fluid passing through to collapse the entire structure. Therefore, the design of the cement must be such that it prevents:

- Micro-annuli formation
- Stress cracking
- Corrosive fluid invasion
- Fluid migration
- Annular gas pressure

In HPHT cases, we need more flexible cement than in conventional wells. This cement expands more at least 2 to 3 times more in some special cases.

The stress in the cement is strongly connected with temperature and pressure, as well as lithology and in-situ stress. If we can define a method which connects the higher temperature to the lower stress field, we would have the solution for one side of the equation, and then we could model the pressure (stress principles) at the designated depth and lithology. Since the stress is so dependent on temperature, the temperature variation must be accurately predicted to properly design the fluid and eliminate excessive time spent waiting on cement. In addition, a post-job analysis is necessary to ascertain zonal isolation and avoid unnecessary remedial work.

By increasing the flexibility of the set cement (lowering the Young's modulus), we can reduce the tensile stress in the cement sheath during thermal expansion. This could be a solution to the problem of cement stability in high temperature cases.

Here we report the use of the finite-element method (FEM) to investigate the stress fields around and inside the cement, and to forecast the time of failure and its affect on cement integrity. This method is more powerful than conventional stability methods since complex boundary conditions are involved as initial conditions and are investigated simultaneously to more accurately predict cement failure.

The results of this study show the relevant dependency of stress principles with temperature and pressure. These results clarify the deformation caused by any disturbance in the system and the behavior of under-stress locations based on their relative solid properties.

DEDICATION

To my father, Mohammad Ali
To my mother, Zahra
To my brothers, Abbas & Hossein
To my sister, Fatemeh

ACKNOWLEDGMENTS

I would like to take this opportunity to express my sincere appreciation to the people who have assisted me throughout my studies.

I would specifically like to thank my advisor, Dr. Jerome J. Schubert, for his guidance and encouragement throughout my research. His patience over the period of my research is also gently appreciated.

I would also like to acknowledge Dr. Hans C. Juvkam-Wold and Dr. Reza Langari for their participation in my research as members of my advisory committee.

I greatly appreciate the considerable attention of Dr. James E. Russell.

I greatly appreciate the help of Mr. Reza Karimi, Ph.D. student in Aerospace Engineering, for his invaluable time and patience regarding the learning of ANSYS.

I also gently appreciate the attention of Dr. Tom A. Blasingame for selecting me as an Aggie and guiding me through my graduate studies.

Finally, I want to really thank all my friends in this department for making my graduate years pleasant and effective.

TABLE OF CONTENTS

Page

LIST OF FIGURES

FIGURE Page

LIST OF TABLES

CHAPTER I
INTRODUCTION

High-pressure/high-temperature reservoirs generally exhibit the following characteristics: Pressure greater than 1000 bar or mud weight more than 16 pound per gallon (ppg), temperature higher than 160^0 C, and total vertical depth greater than 4500 m.

Set cement behavior is very different than while in the slurry state. Since slurry is still in fluid mode, it should be investigated by studying the fluid rheology; after a certain amount of time, it will set up to form a solid material. Slurry behaves like a visco-plastic material since changes in the cement properties are irreversible while the cement hardens.

While the slurry sets, the cement behavior is governed by the chemical reduction of its components. Young's modulus and Poisson's ratio will describe the cement behavior under different stresses.

The goals in this research are as follows:

- Find the pressure and temperature distribution profiles in the system.
- Relate this distribution to physical rock properties of cement, casing and formation.
- Determine the time and conditions of cement failure

Permeability shrinks greatly at higher temperature, and since the relative permeability of the rock is a temperature-dependent factor,[1] it is very important to watch permeability reduction in cement both short term and long term.

Rock mechanics is the subject concerned with engineering disturbance.[2] Thus rock mechanics may be applied to many engineering applications ranging from dam abutments, to nuclear power station foundation, to the manifold methods of mining ore and aggregate materials, to the stability of petroleum wellbores, and including newer applications such as geothermal energy and radioactive waste disposal.

1.1 Importance of Primary Cementing on Cost

Avoiding remedial cementing operations is one of the most important objectives during cementing operations. Remedial operations can pose extreme risks and high associated costs.

This thesis follows the style and format of *SPE Drilling & Completion*.

Completions in HPHT reservoirs remain very expensive even without including remedial cementing and logging. High cost makes it necessary to cement the casing successfully on the primary cement job, eliminating the need for remedial cementing. Equipment improvement aims to reduce times for testing, placement, cement bond logging (CBL), and equipment use.

In cases of narrow margin between pore pressure and fracture pressure, the increase in mud density can induce lost circulation and can further reduce the chance for a successful cementing job. Mud properties become vital in ensuring the best conditions for cementing, in terms of both reduced equivalent circulating density (ECD) and desired mud properties for cementing, and they have been crucial in the success of cementing operations.

1.2 Wellbore Temperature

Monitoring wellbore temperature is one of the most important factors controlling the chemical reaction and performance results of a cementing operation.[3] In oil/well cementing, the cement slurry placed at total depth is subject to progressively increasing temperature from the time it is mixed on the surface and pumped into the well until the time the cement cures and the formations adjacent to the wellbore return to their ultimate static pressure. Circulating and static temperatures both affect cement design. Circulating temperature is the temperature the slurry encounters as it is being pumped into the well. Static temperature is the formation heat to which the slurry will be subjected after circulation is stopped for a set period of time. Although static temperatures affect the curing properties of the cement, circulation temperature has an even greater impact.

Bottomhole circulating temperature (T'_c) is the temperature that influences the thickening time or pumpability of the cement slurry. T'_c is usually calculated form a set of schedules published in API RP 10B.[4]

Designers should know the bottomhole static temperature (T'_s) to design and assess long-term stability, or rate of compressive strength development for the cement slurry. Determining T'_s is especially important in deep well cementing, where the temperature differential between the top and bottom of the cement can be great. Generally, cement sensitivity increases as the T'_s increase.

1.3 Cement Slurry Sensitivity With Temperature

Temperature has a profound effect on the safe placement of the cement slurry.[5] Under normal cementing conditions for vertical wells, API tables and calculations have been used successfully for many years. However, for HPHT wells, the high temperatures cause the slurries to be even more sensitive to temperature and, therefore, the accuracy of the predicted cementing temperature is more critical. Also, because of the depth of the casing string, cementing volumes and displacement times are greater than normal. This increases the acceptable thickening time required for safe placement. Therefore, more retarder is required for HPHT cases. If the cement is over-retarded, compressive-strength development may take longer than required. This over-retardation may also be a detriment to other properties such as the slurry's resistance to gas migration.

1.4 Gas Migration

Avoiding gas migration in a cemented annulus is one of the problems to be overcome in well cementing.[6] The main reason for this is the cost of the well. Gas can migrate through cement while the cement is setting and the slurry is in the fluid form. If volume contraction of fluid loss is relevant, the room for the gas to invade is being provided. In this case special additives such as permeability reducers and volume expanders can be useful in avoiding gas intrusion, and the slurry gelation will impede hydrostatic pressure transmission and reduce pressure in front of the gas zone. Finally, the cement reaches the state of an impermeable solid. Now the solid cement should sustain the thermal shocks as well as production-testing shocks. Besides density control and slurry design, mud-cake and cutting removal is another critical aspect for achieving good zonal isolation.

To remove the mud cake and cuttings, it is better to apply a high-velocity cement profile (flattened profile, **Fig. 1.1a**) which results in higher velocity on the boundaries (wall of the well) and removes the cuttings more effectively than laminar flow (elongated profile, **Fig. 1.1b**). Optimizing slurry design is essential with zero free water; minimum fluid loss and difference between the times for reaching 50 and 100 consistency units under 10 minutes are desirable. The fast development of gel and the

maintenance of gel strength below 100 $lb_f/100ft^2$ until thickening time is the most important parameter to be achieved.

Following are some cementing samples which did not resist gas migration and as a consequence, the gas penetrated the cement all the way up and caused borehole damage during production pressure tests. **Figs. 1.2 to 1.3** show the gas damage (severe or partial) to the cement from channeling.[7] In the most severe case, we can look forward to the casing corrosion from the formation gas. **Fig. 1.4** relates the de-bonding and micro-annular forming in the cement, which can let gas migrate through and result in sustained casing pressure.

a b

Fig. 1.1− High-velocity flow (a) removes cutting better than laminar flow (b)[7]

Fig. 1.2− Severe gas channeling [7]

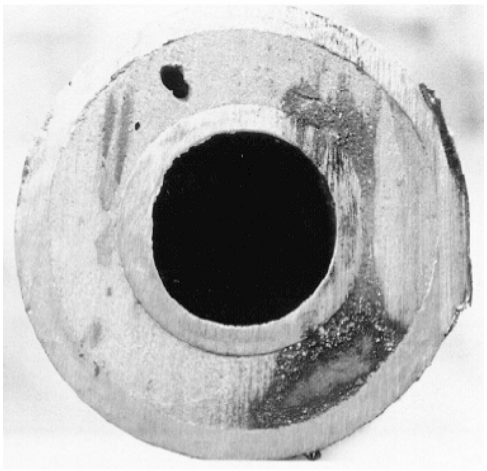

Fig. 1.3− Gas channeling [7]

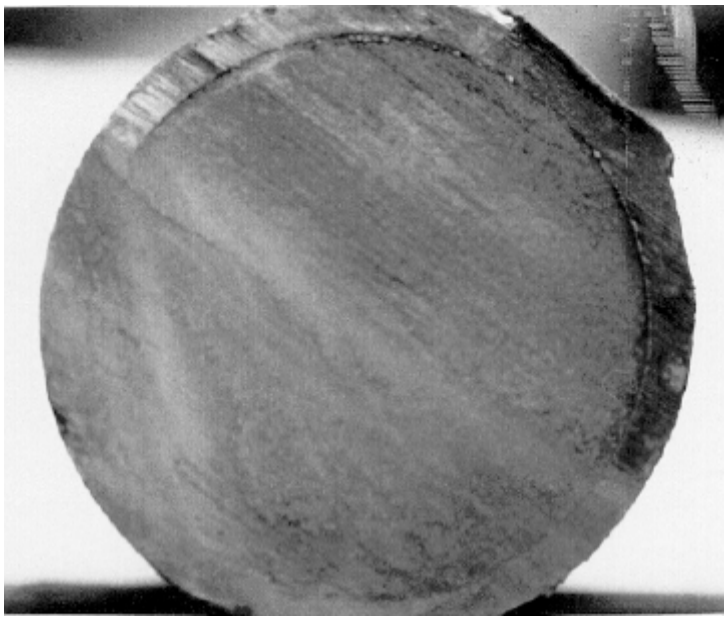

Fig. 1.4− Micro-annulus gas migration [7]

CHAPTER II

FINITE-ELEMENT ANALYSIS

2.1 What Is Finite-Element Analysis?

Finite-element analysis (FEA) is a tool to better understand how a design will perform under different sets of impacts or stresses in certain conditions. FEA is a computer-based mathematical representation method of solving problems numerically. Since this a numerical solver, the answer is not exact. It works on the basis of material properties, type of model, and boundary conditions. Applicable boundary conditions instead of random boundary condition would affect the results very much and could result in early model collapse.

Each finite-element (FE) simulator has three sections. In the first part, which is the pre-processor, we generate the model and try to define it with some input. These inputs include data for type of materials used in the model, applicable boundary conditions, applicable type of element (which is highly dependent on type of investigation), number of nodes, type of meshes, and the tolerance between the nodes and the elements. (Elements are different from meshes)

For example, if the system is symmetric, it is better to apply a mapped mesh configuration; where-as, when the shape is of uncertain geometry, it is better to let the system apply free meshes. Since we are attempting to get the results faster, applying related elements governing relevant partial differential equations is inevitable. For 2D analysis, usually requires apply a quadratic-element with eight nodes for civil and construction engineering. The main reason for choosing this element type is that first, the system has to solve a second- order partial differential equation, and second, because it is faster than complicated elements and, in its category, is a lot better than triangular six node elements or quadratic-element with four nodes. This system of quadratic-elements with eight nodes is mostly applicable for plane-stress or plane-strain investigations.

In the second part, which is the processor, the system runs the input data to match the best fit as the final results. This section, which is called the solver, performs most of the work.

Finally in the third part, which is known as the post-processor, we can see the behavior of the model under certain conditions that are defined in the pre-processor.

We define the finite-element process as any approximation process in which:

- The behavior of the whole system is approximated to by a finite number, *n* of parameters, a_i, *i*=1 to *n*.
- The n-equations governing the behavior of the whole system can be assembled by the simple process of addition of terms contributed from all sub domains (or elements) that divide the system into physically identifiable entities[8] without overlap or exclusion.

Griffith[9] discussed finite-element analysis used by Halliburton Co. to design cementing for HPHT wells, using examples from Brazil, West Africa, and the Gulf of Mexico. Griffith also described best practices that should be used to successfully isolate zones in harsh downhole conditions.

2.2 How Is Finite-Element Analysis Useful?

Since FE is a simultaneous multi-partial-differential equations solver, it is a time saver. Without applying FE, civil engineering would never be able to reach to the goals it can today. FE can handle complex boundary condition; that's why we still use this type of programming for investigating problems more realistically than the finite difference method (FDM). FE application is mostly for solid mechanics, but FDM can be used better in the field of fluid mechanics and hydraulics.

2.3 What Are the Differences of FEM and FDM?

FDM works basically on nodes and the relation between nodes. It is a lot faster than FEM in this case, but it can not tolerate complex boundary-condition problems and it is mostly used in fluid behavior modeling. FEM can tolerate the most complex boundary conditions but is not as fast as FDM. In FEM, elements do the job of nodes in FDM. FEM is mostly used for solid mechanics and it is applicable for visco-plastic and visco-elastic media. (Visco-elastic media refers to those media which are reversible with time, and visco-plastic refers to those media which are irreversible with time)

CHAPTER III

MECHANICAL AND THERMAL PROPERTIES OF ROCKS AND CEMENT (STATIC AND DYNAMIC)

3.1 Mechanical Properties of Rock

Set cement behavior is very similar to rock behavior, so, we can apply the same principles to both with different parameters. Eqs. 3.1 – 3.7 are the main and principle formulas in rock mechanics analysis and can be applied to different media (rock, cement, and steel).

Poisson's ratio is a constant which determines type of rock or matrix and can be easily calculated by applying Eq. 3.1 R_v is just the ratio of shear-wave travel time to compression-wave travel time and is represented in Eq. 3.2.

$$\nu = \frac{0.5R_v^{\,2} - 1}{R_v^{\,2} - 1}, \quad \text{..... (3.1)}$$

where, ν = Poisson's ratio

$$R_v = \frac{\Delta t_s}{\Delta t_c} = \frac{v_c}{v_s}, \quad \text{..... (3.2)}$$

where, Δt_s = shear-wave travel time
Δt_c = compression-wave travel time
v_c = compression-wave velocity
v_s = shear-wave velocity

The shear modulus is defined as the ratio of shear stress to engineering shear strain on the loading plane. (Eq. 3.3)

$$G = 1.34\times10^{10}\rho_b / \Delta t_s^{\,2} \quad \text{..... (3.3)}$$

where, G = Shear modulus
ρ_b = bulk density

Young's modulus is basically the ratio of stress to strain, and Eq. 3.4 shows another form of Young's modulus, the dynamic Young' modulus, which is variable with different media or matrices. The relation between the static Young's modulus (E_s) and dynamic Young's modulus (E_d) is presented through Lacy's correlation. (Eq. 3.5)

$$E_d = 2G(1+\nu), \quad \text{(3.4)}$$

$$E_s = 0.018E_d^{\,2} + 0.4224E_d, \quad \text{(3.5)}$$

The bulk modulus gives the change in volume of a solid substance with a change in applied pressure. (Eq. 3.6)

$$K = 1.34\times10^{10}\rho_b\left(\frac{1}{\Delta t_c^{\,2}} - \frac{4}{3\Delta t_s^{\,2}}\right), \quad \text{(3.6)}$$

where, K = bulk modulus

The *in-situ*, minimum horizontal stress ($\sigma_{h,\min}$) can be calculated with Eq. 3.7. The *in-situ* stress is highly dependent on rock pore pressure and overburden pressure. Tectonic stress has some effect on this stress but it is not considerable. (We may measure *in-situ* stress with the correction for tectonic stress from log data)

$$\sigma_{h,\min} = \sigma_x = \left(\frac{\nu}{1-\nu}\right)(\sigma_z - P_p) + P_p + \sigma_{tec}, \quad \text{(3.7)}$$

where, $\sigma_z = \sigma_{ob}$ = overburden stress
P_p = pore pressure
σ_{tec} = tectonic stress

Table 3.1 shows some deterministic properties of different lithologies and fluid saturations based on the ratio of shear-wave travel time to compressional travel time.

TABLE 3.1− Lithology Determination Based on Travel Time Ratios[10]

Lithology	$\Delta t_s / \Delta t_c$
Sandstone/Water	1.78
Sandstone/Gas	1.60
Dolomite	1.80
Limestone	1.90

3.2 Calculation the Effect of Temperature

Heat transfer to the casing will occur by conduction, convection, and radiation. Huygen and Huitt[11] showed that radiation accounts for two-thirds of the heat loss, while convection plays a very small role. (In the following discussion, I shall neglect

convection as a heat-loss mechanism). If the casing temperature is T_c in ^oF (or ^oC), and the thermal conductivity of the annulus fluid is K_{hf} in Btu/hr-ft-^oF (KW/m-K), then the conduction (q) and radiation heat loss is given by Eq. 3.8:

$$q = \frac{2\pi K_{hf}(T_s - T_c)}{Lnd_{ic}/d_{ot}} + \pi d_{ot}\Sigma\sigma'(T_s^{\,4} - T_c^{\,4}), \quad \text{..... (3.8)}$$

where, T_c= casing temperature

K_{hf} = thermal conductivity of the annulus fluid

T_s= surface temperature

d_{ic}= inside casing diameter

d_{ot}= outside diameter

σ' = conversion factor

Σ = view factor

In Eq. 3.8, the conversion factor $\sigma' = 0.1713 \times 10^{-8}$ for British units and $\sigma' = 5.66 \times 10^{-11}$ for SI units, and the view factor Σ, is given by Eq 3.9:

$$\frac{1}{\Sigma} = 1 + (\frac{1}{\varepsilon_{to}} - 1) + (d_{ot}/d_{ic})(\frac{1}{\varepsilon_{ci}} - 1), \quad \text{..... (3.9)}$$

where, ε_{ci} = emissivity of the casing interior

ε_{to} = emissivity of the casing exterior

The term "emissivity" mostly applies to the surface and it means the amount of energy emitted through the surface that is perpendicular to the flow direction. In the case of surface pipe, ε'=0 for a perfectly reflecting surface, while ε'=1 for a black body. The heat loss from the casing exterior to the surrounding soil, initially at a formation temperature T_f is time-dependent and takes place by conduction. It is given by Eq. 3.10. in this equation K_{hob} is thermal conductivity of the adjacent media, T_f is the formation temperature, d_{oc} is the outside casing diameter, α is the thermal conductivity of the media, and t is the time.

$$q = \frac{4\pi K_{hob}(T_c - T_f)}{Ln16\alpha t/d_{oc}^{\,2} - 0.5772}, \quad \text{..... (3.10)}$$

3.3 Heat Flow in Cement

Since the thermal conductivity of cement is about one-third of the surrounding earth, the insulating effect of cement around the casing is important. In such an instance, let T_{cem} be the temperature of cement and K_{hcem} the thermal conductivity of cement in Btu/hr-ft-^{o}F (KW/m-K). Also, let the external diameter of the cement covering be d_{cem} in ft (m). Again, to allow for heat transfer resistance through the casing steel wall, calculate the overall heat transfer coefficient U given by Eq. 3.11: [12]

$$U = \left(\frac{d_{cem} Lnd_{cem} / d_{oc}}{2K_{hcem}} + \frac{d_{cem} Lnd_{oc} / d_{ic}}{2K_{hs}}\right)^{-1}, \quad \text{(3.11)}$$

Then T_{cem} is given by Eq. 3.12:

$$T_{cem} = T_c - q/(\pi d_{cem} U), \quad \text{(3.12)}$$

For this case replace T_c by T_{cem}. Thus, we introduced one additional unknown, T_{cem}, which can be obtained from Eq. 3.11.

3.4 Fourier's Law of Heat Conduction

This paper uses two forms of Fourier's law, one linear and one dimensional. The formula is represented in Eq. 3.13, where q_h is the heat conduction and $\frac{dT}{dz}$ is the thermal gradient.

$$q_h = -k_h \frac{dT}{dz}, \quad \text{(3.13)}$$

Values of thermal conductivities are shown below on **Table 3.2.**

Be aware that thermal conductivity is not always constant; it frequently changes with temperature.

TABLE 3.2 − Thermal Conductivity of Selected Material[10] (10^{-3} cal/ (sec-cm-^{o}C))

Shale	2.8 to 5.6
Sand	3.5 to 7.7
Porous limestone	4 to 8
Dense limestone	6 to 8
Dolomite	9 to 13
Quartzite	13
Gypsum	3.1
Anhydrite	13
Salt	12.75
Sulphur	0.6
Steel	110
Cement	0.7
Water	1.2 to 1.4
Air	0.06
Gas	0.065
Oil	0.35

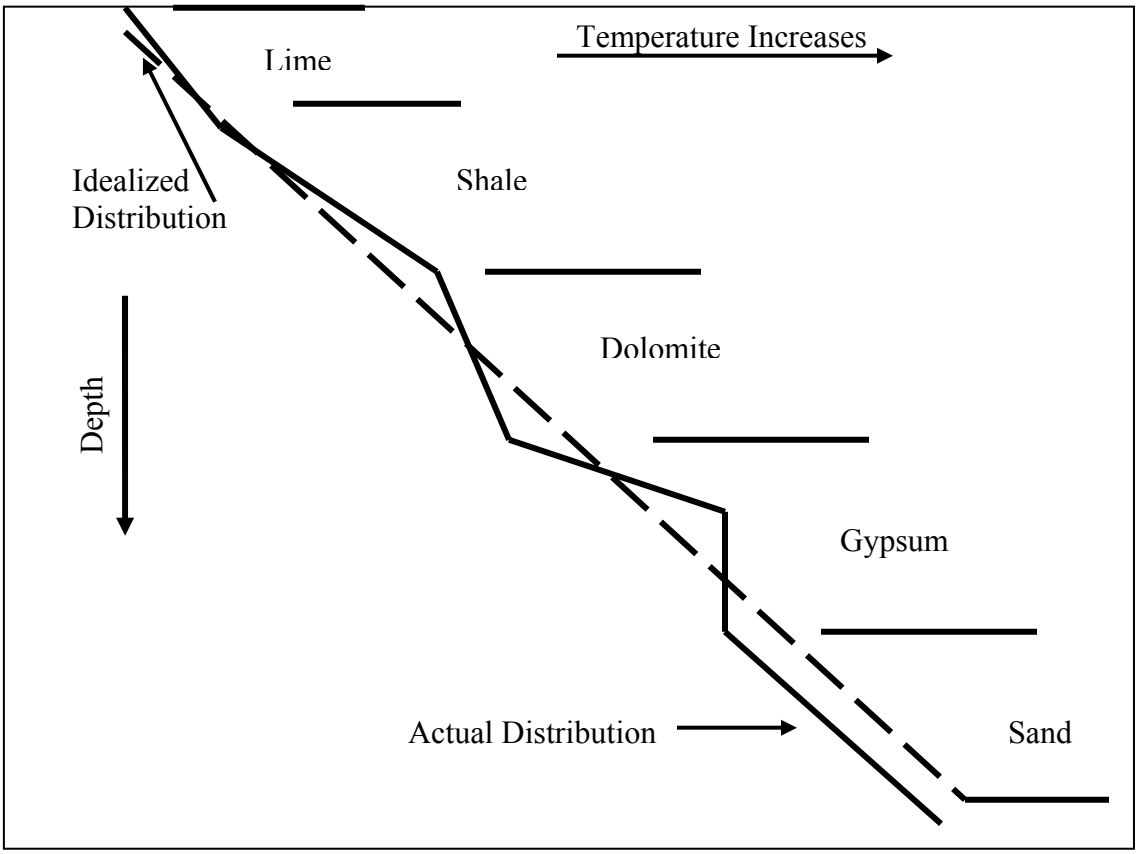

Fig. 3.1− Actual and idealized subsurface temperature distribution [10]

A semi-log plot of temperature data obtained in wells drilled in Pecos County, Texas, is shown in **Fig. 3.1**. Eq. 3.14 demonstrates the relation of formation temperature and surface temperature, where m_f is constant.

$$T_f = T_s \exp(m_f D), \quad \text{..... (3.14)}$$

where, D= depth

We conclude that the temperature gradient is not always linear, particularly for greater depths. Fourier's second order law of heat conduction can be written as Eq. 3.15. If we expand this temperature distribution formula for our setup in a steady state system, since no heat is generated or lost, the right side of equation will be equalized to zero in Eq. 3.16. In this equation, ∇T is the temperature operator in the media, ρ is the density of the media, and ϕ is the porosity of the media.

$$K\nabla^2 T = -\rho\phi, \quad \text{..... (3.15)}$$

$$\frac{\delta^2 T}{\delta r^2} = 0, \quad \text{..... (3.16)}$$

Solving Eq. 3.16 for the temperature distribution with radius will result in Eq. 3.17.

$$T(r) = C_1 r + C_2, \quad \text{..... (3.17)}$$

To solve this equation, we have to apply relevant boundary conditions. According to **Fig. 3.2,** the boundary conditions for this case can be shown by Eq. 3.18 and Eq. 3.19.

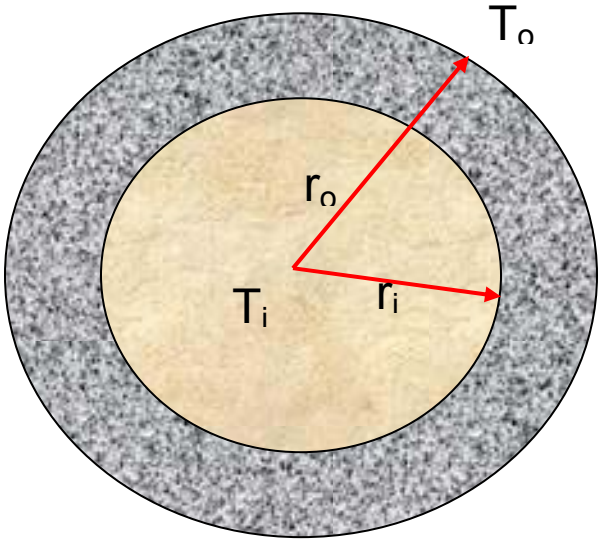

Fig. 3.2– Schematic of wellbore and cement

Boundary conditions for this system are as follows:

$$T(r_i) = T_i \ @ \ r = r_i, \quad \text{(3.18)}$$

$$T(r_o) = T_o \ @ \ r = r_0, \quad \text{(3.19)}$$

Solving Eq. 3.17 with the boundary conditions in Eq. 3.18 and 3.19 would give the solution to temperature distribution in this system. We can find the amount of constants from Eq. 3.17.

After solving Eq. 3.17 through Eq. 3.19 for C_1 and C_2, we can write Eq. 3.20 and Eq. 3.21 for these two constants as follows:

$$C_1 = \frac{T_o - T_i}{r_o - r_i}, \quad \text{(3.20)}$$

$$C_2 = \frac{T_i(r_o - r_i + 1) - T_o}{r_0 - r_i}, \quad \text{(3.21)}$$

If we complicate the scenario as shown in **Fig. 3.3**, we can simulate the temperature behavior through this system more idealistically.

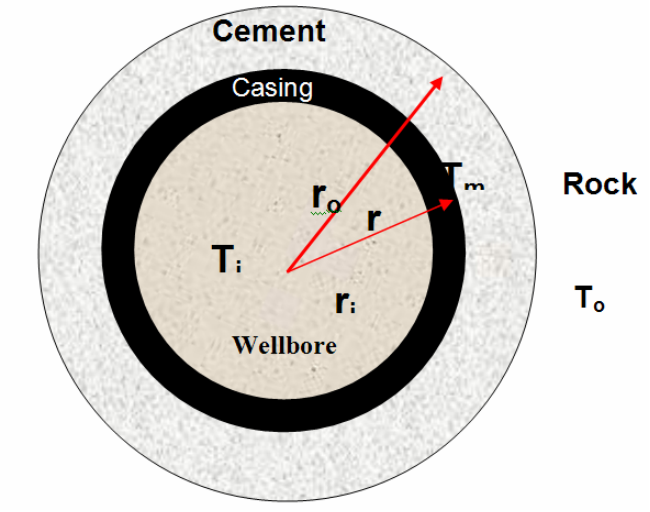

Fig. 3.3− Schematic of wellbore, casing, cement, and rock

Developing the relative formula, Eq. 3.16, for the newer case is exactly the same as before, but since the boundary conditions change, we have two basic formulas (Eq. 3.22 and Eq. 3.23) with four unknowns that will be determined with various boundary conditions. The new boundary conditions are summarized in Eq. 3.24 to Eq. 3.27.

$$T_s(r) = C_1 r + C_2 , \quad \text{(3.22)}$$

$$T_c(r) = C_3 r + C_4 , \quad \text{(3.23)}$$

$$T_s(r_i) = T_i \ @ \ r = r_i , \quad \text{(3.24)}$$

$$T_c(r_o) = T_o \ @ \ r = r_0 , \quad \text{(3.25)}$$

$$T_s(r_m) = T_c(r_m) \ @ \ r = r_m , \quad \text{(3.26)}$$

$$q_s(r = r_m) = q_c(r = r_m)$$

$$K_s \frac{dT_s}{dr}(r = r_m) = K_c \frac{dT_c}{dr}(r = r_m) , \quad \text{(3.27)}$$
$$K_s C_1 = K_c C_3$$

Eq. 3.27 is the result of continuum theory. In this theory, the temperatures, in two adjacent elements are equal. The constants in Eq. 3.22 and Eq. 3.23 can be explained in Eq. 3.28 to Eq. 3.31.

$$C_1 = \frac{T_C - T_S}{(r_m - r_i) + \frac{K_s}{K_c}(r_0 - 1)} , \quad \text{(3.28)}$$

$$C_2 = T_s - \frac{(T_c - T_s) r_i}{(r_m - r_i) + \frac{K_s}{K_c}(r_o - 1)} , \quad \text{(3.29)}$$

$$C_3 = \frac{\frac{K_s}{K_c}(T_c - T_s)}{(r_m - r_i) + \frac{K_s}{K_c}(r_o - 1)} , \quad \text{(3.30)}$$

$$C_4 = T_c - \frac{\frac{K_s}{K_c}(T_c - T_s)r_o}{(r_m - r_i) + \frac{K_s}{K_c}(r_o - 1)}, \quad \text{(3.31)}$$

Now, with these sets of equations we can model any situation which can possibly occur in the wellbore area. Note that these equations are derived in the steady-state case and derivation for unsteady-state requires a higher degree of mathematics. With these equations, we can calculate the constants and solve the equations easily, then expand the criteria to other properties of wellbore.

CHAPTER IV

MECHANICAL AND THERMAL STRESSES

4.1 Stress

Stress is a concept which is fundamental to rock mechanics principles and applications. Stress is not scalar nor vector; it is a tensor, which means it has quantity with magnitude and direction in the plane under consideration.[2]

4.2 Mohr's Circle

Mohr circle is a plot of stability between shear-stress versus normal stress. This semigraphical procedure is used to better understand the analysis of plane-stress problems.

We can generate this circle from σ_x, σ_y, and shear-stress, τ_{xy}. Eq. 4.1 calculates the center, C, of the circle; Eq. 4.2 constructs the required radius, r, of the circle.

$$C = \frac{\sigma_x + \sigma_y}{2} \quad \text{..... (4.1)}$$

$$r = \frac{\sigma_x - \sigma_y}{2} = \sqrt{(\frac{\sigma_x - \sigma_y}{2})^2 + \tau_{xy}^2} \quad \text{..... (4.2)}$$

Maximum (σ_1) and minimum (σ_3) stresses can be calculated through Eq. 4.3.

$$\begin{aligned} \sigma_1 &= C + r \\ \sigma_3 &= C - r \end{aligned} \quad \text{..... (4.3)}$$

From Eq. 4.1 and Eq. 4.2 and **Fig. 4.1**, we can calculate maximum and minimum stresses and shear stress. Eq. 4.3 and Eq. 4.4 calculate the normal stress and shear stress respectively.

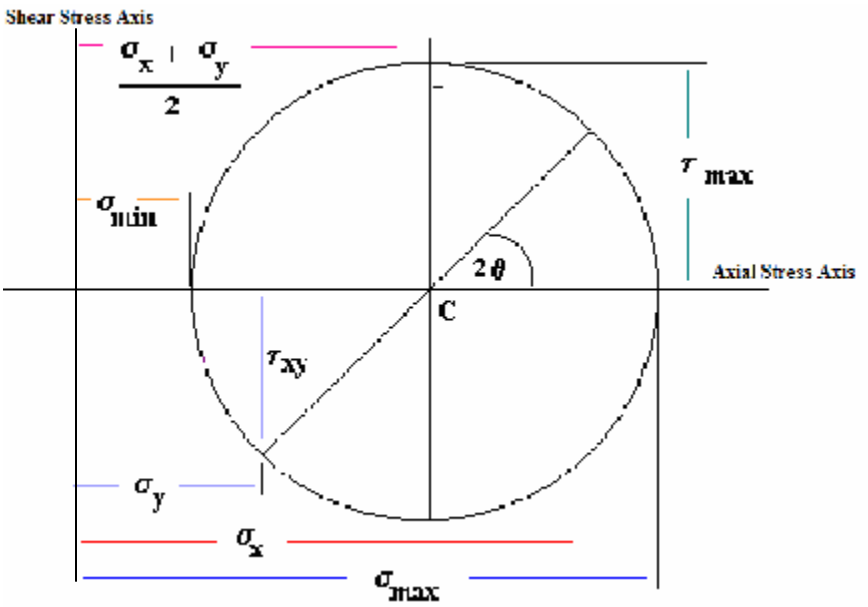

Fig. 4.1− Mohr's circle

$$\tau_{xy} = \frac{\sigma_x - \sigma_y}{2} \sin 2\theta \ , \quad \text{..... (4.4)}$$

where, $2\theta =$ the angle between maximum stress and horizontal line

4.3 Tectonic Stress

We can calculate the in-situ stress ignoring the tectonic stress. But in the real world, tectonic stress originated with plate tectonics. Because of tectonic stress, each part of the lithosphere has a certain amount of stress relevant to its nature. Local loading such as thermo-elastic loading can not be categorized as tectonic stress. Plate tectonics controls the paleo-stresses (past stresses) in the lithosphere. Paleo-stresses control the direction and magnitude of the fractures and joints in the subsurface. Joints where originated by paleo-stresses can grow with in-situ stresses or non tectonic manners like erosion or local loading.

4.4 Coulomb Failure Criterion

Structural geology is the science of rocks through stresses and deformations. Each deformation will lead to some acting stresses. Since each type of rock will accept some amount of stress and strain before entering another (plastic zone of behavior), mapping the behavior will open new understanding about rock behavior.

Hook's law will clarifies the rock behavior on the basis of its solid mechanical characteristics. For linear elastic behavior, Young's modulus (E) can be calculated with Hook's law through Eq. 4.5. Elastic behavior means once the stress is removed, the body returns to its original shape.

$$E = \frac{d\sigma}{d\varepsilon} \quad \text{..... (4.5)}$$

where, $\sigma =$ active stress on the body

$\varepsilon = \frac{dl}{l}$ = strain or resultant shape change based on active forcing stress, l=length

After a certain amount of stress acts on a rock, the rock will deform. The point of irreversible deformation is called the *yield point*. After the yield point, the rock behavior is no longer elastic. It may become brittle, or ductile, where under additional stress the rock behaves like an elasto-plastic material. In higher quantities of induced stresses, the rock may behave plastically, and at still higher stresses it will break.

The effect of the surrounding rock in the earth is to confine the volume in question and apply a confining pressure (sometimes called a lithostatic stress). In order for rock deformation to take place, the principal stress in one direction (σ_1) must exceed the other two principal stresses (σ_2, and σ_3) which are at right angles to σ_1. This difference between σ_1 and, say, σ_3 is called the differential stress to which the sample is subjected. In the analysis of rock deformation σ_3 is equivalent to the confining pressure.

Our knowledge of the behavior of rocks comes from experiments in the laboratory. One common rock mechanics experiment uses a cylinder of rock placed in a rock-deformation machine. Such a cylinder is shown in cross section in **Fig. 4.2**. Pistons contact the end of the cylinder and create the stresses necessary to deform the rock. The cylinder is surrounded by a confining medium which is prevented from flowing into the pores of the rock sample by an impermeable jacket. In **Fig. 4.2** the sample is stippled, the confining medium is represented by the inward pointing arrows, and the loading pistons are shown as the darker objects on either end of the rock sample. The application of differential pressure is shown by the dark, vertical arrows on either end of the piston.

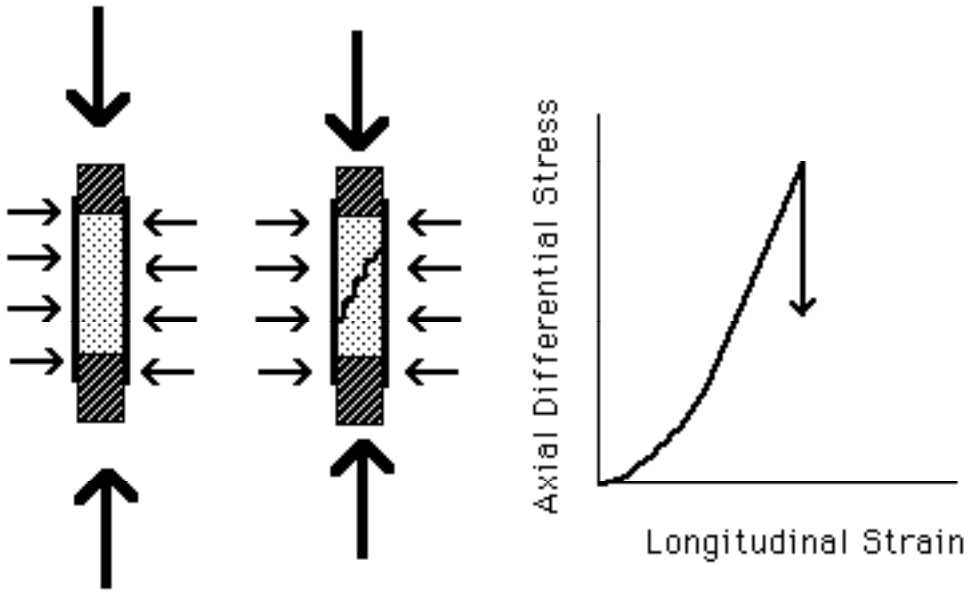

Fig. 4.2− Laboratory stress-strain test[2]

A typical stress-strain curve is shown to the right of the rock-deformation experiments. As stress increases on the rock, the rock strains. Once the fracture strength of the rock is reached, the rock fails along one or more fracture planes (**Fig 4.3**). The failure is denoted by a sudden stress drop in the stress-strain curve.

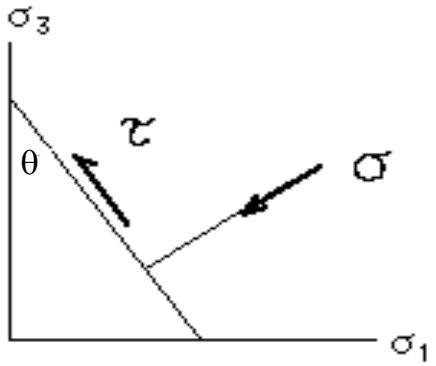

Fig. 4.3− Fracture initiation in the rock[2]

In the late 18th century a French naturalist, Coulomb,[2] observed for rocks that shear stress $|\tau|$ necessary to cause brittle failure across a plane is resisted by the cohesion of the

material, S_o, and by a constant; *μ, times the normal stress, σ_n, across that plane, which may be calculated with Eq. 4.6 as follows:

$$|\tau| = S_o + *\mu\sigma_n, \quad \text{.....(4.6)}$$

The coefficient of internal friction,*μ, is not to be mistaken for μ, the coefficient of sliding friction. Because a shear stress was parallel to the plane of failure, the brittle fracture is commonly called a shear fracture. This mode of fracture should be distinguished from a tensile crack that opens normal to the least principal stress (σ_3).

4.5 Thermal Stresses

Usually the bottomhole injection temperature of the treating fluid differs from the initial reservoir temperature.[12] With this differential temperature, thermal stresses are induced in the formation during hydraulic fracturing. For a temperature change, Δθ, the volumetric strain, Δe_s and Δe_f, in the elements of the rock and fluid are, respectively,

$$\Delta e_s = \alpha_s \times \Delta\theta, \quad \text{..... (4.8)}$$

where, Δθ= Temperature change

α_s= Volumetric coefficient of thermal expansion of the rock

$$\Delta e_f = \alpha_f \times \Delta\theta, \quad \text{..... (4.9)}$$

where, α_f= Volumetric coefficient of thermal expansion of the fluid

The change in stress fields caused by change in temperature in an elemental sphere of the poro-elastic solid can be obtained by using the concept of transformation strain introduced by Eshelby.[13]

Laboratory measurements[14] show that shale has a higher Poisson's ratio and a lower Young's modulus than sandstone from the same reservoir. The area of lower Poisson's ratio is the area of fracture height extension, and increased values represent a barrier of vertical fracture extension. Wherever the Poisson's ratio value is high, the fracture extension stops. From spontaneous potential (SP) logs and resistivity logs, we can anticipate the fracture trend and its possible deviations. The highest Poisson's ratio value is used to determine the fracture height.

The essential factors for fracture propagation are:

- material properties in the pay zone and in the barrier zone

- In-situ stress in the pay zone and in the barrier zone
- Effect of hydrostatic pressure gradient

The fracture height determination method[15] can be used in determining the location of formation failure during cementing, drilling, killing the well , and when formation fracture causes lost circulation. Because of fluid migration and heat transfer in the reservoir, such differential temperature induces thermal stresses. Mechanical properties needed to model the fracture include minimum horizontal in-situ stress, fluid leak-off coefficient, elastic modulus, Poisson's ratio, and fracture toughness.

4.6 Mechanical Stresses on the Cement-Casing System and Related Calculations

According to **Fig. 4.4,** two types of stresses affect casing and cement. These two types can be summarized as radial stresses and tangential stresses. The magnitude of each of these two types can vary with different situations.

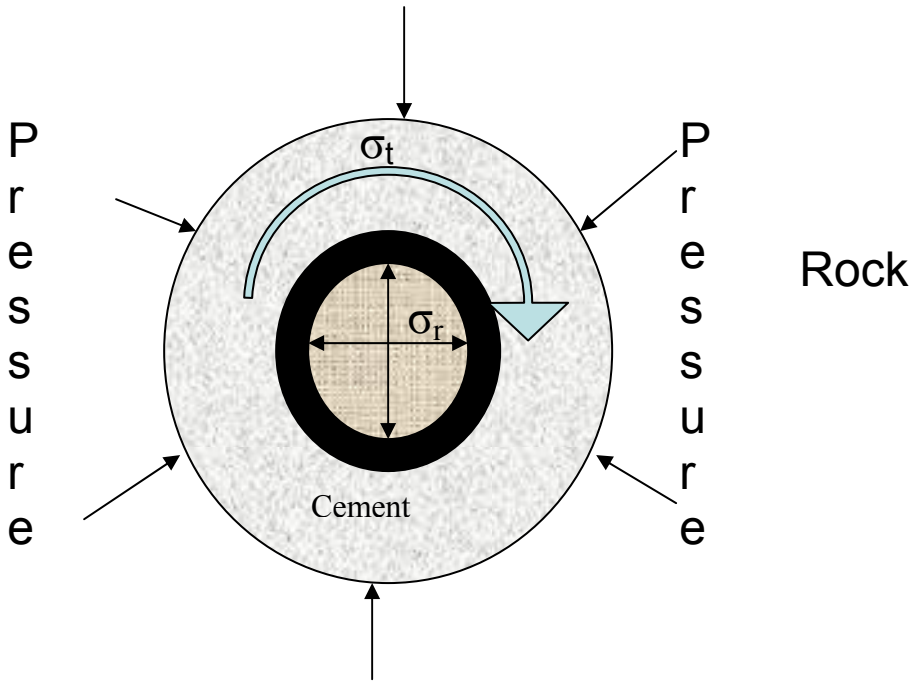

Fig 4.4− Schematic of stresses exerted on wellbore

According to **Fig. 4.5,** the pressure inside the wellbore and in the formation is a depth variable function, and should be considered.

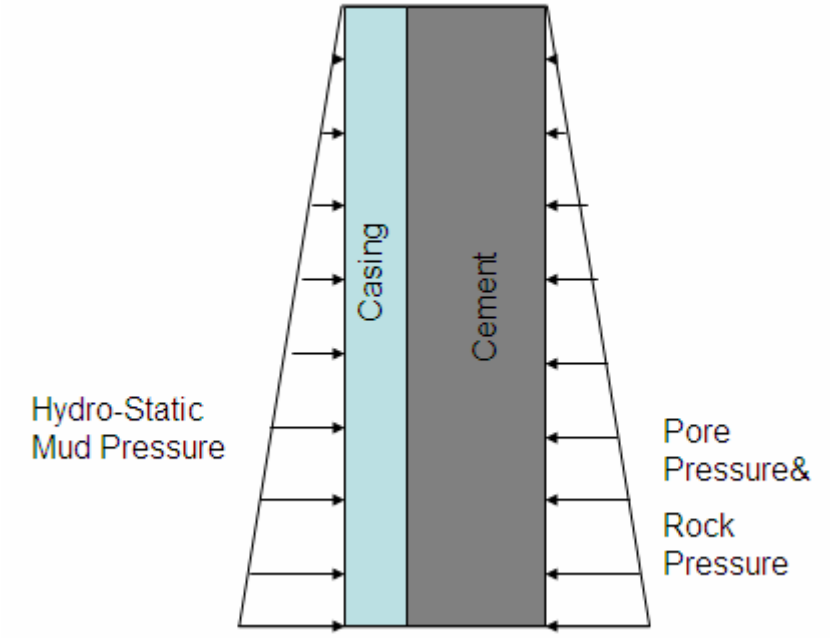

Fig. 4.5− Schematic of pressures around and inside the wellbore

The value of hydrostatic pressure inside the wellbore can be directly calculated with Eq. 4.10. In the outer boundary we encounter two types of pressures, the rock pore pressure and the overburden pressure. The result of these two pressures is the in-situ pressure, which acts horizontally toward the wellbore and is shown in Eq. 3.7.

$$P_{Hyd} = 0.52 \times \rho_{mud} \times TVD \,, \quad (4.10)$$

where, P_{Hyd}= hydrostatic pressure

TVD= total vertical depth

We can calculate the amounts of radial stress and tangential stress in the cement and casing with Eq. 4.11 to Eq. 4.12.

$$\sigma_r = \sigma_H (1 - \frac{r_w^{\,2}}{r^2}) + \frac{r_w^{\,2}}{r^2} P_w \,, \quad (4.11)$$

where, σ_r = radial stress

r_w = wellbore radius

and $P_w = P_{Hyd}$

$$\sigma_t = \sigma_H (1 - \frac{r_w^{\,2}}{r^2}) - \frac{r_w^{\,2}}{r^2} P_w \,, \quad (4.12)$$

where, σ_t = tangential stress

Solving those equations with certain assumptions such as, no shear on the wellbore wall and rotational symmetry, we arrive at Eq. 4.13 and Eq. 4.14, which are the results used in this study.

$$\sigma_r = \frac{E}{(1+\nu)(1-2\nu)}\left[C_1 + \frac{C_2}{r^2}(1-2\nu)\right] \text{ , ……..…….. (4.13)}$$

and

$$\sigma_\theta = \frac{E}{(1+\nu)(1-2\nu)}\left[C_1 - \frac{C_2}{r^2}(1-2\nu)\right] \text{ , ……... (4.14)}$$

This derivation is based on the concept of plain-strain, which says that strain along the wellbore axis is zero, and the two horizontal stresses are assumed equal, no tectonic activity which is applicable for Gulf of Mexico.

Since in this case we just consider the horizontal plane and stresses, the function of vertical stress has been ignored.

Obviously each time the in-situ stress acting from the outer boundary and the hydrostatic mud pressure from inner boundary, are unequal, we can have a movement in the structure that will result in the creation of fractures in the cement or collapsing the entire structure. This situation may occur where is a loose, unconsolidated layer, like shale, lies outside the cement.

In our analysis in the next chapter, I fixed the casing structure at some points to prevent the casing from moving while we change pressure on one side. We are simplifying this situation to analyze the stress concentration in the casing/cement system.

CHAPTER V

WELLBORE STABILITY

To minimize the mechanical instability, mud of the right density should be determined. The two main types of rock failure are tensile and compressional (or shear) failure. For these failures to occur, certain criteria must be met. The modes of failure highly depend on the mud weight pressure. Understanding stability provides additional information to analyze drilling events, which allows the alteration of drilling and completion operations.

5.1 Factors Affecting Wellbore Stability

As summarized in **Fig. 5.1**, many factors relate to wellbore stability. Many of these factors are controllable, although a number of them are beyond our control.[16] The formation type, its permeability, presence of fractures, presence and percentage of shale, swelling behavior, in-situ stress, temperature, and rock thermal properties are out of our control and should be balanced through controllable mechanical and chemical properties of drilling mud, type of completion, hole size, and penetration rate. Fluid rheology should be understood quite well in case of washouts through shale in the wellbore wall, and adjacent formation pressures should be reviewed to prevent wellbore breakage.

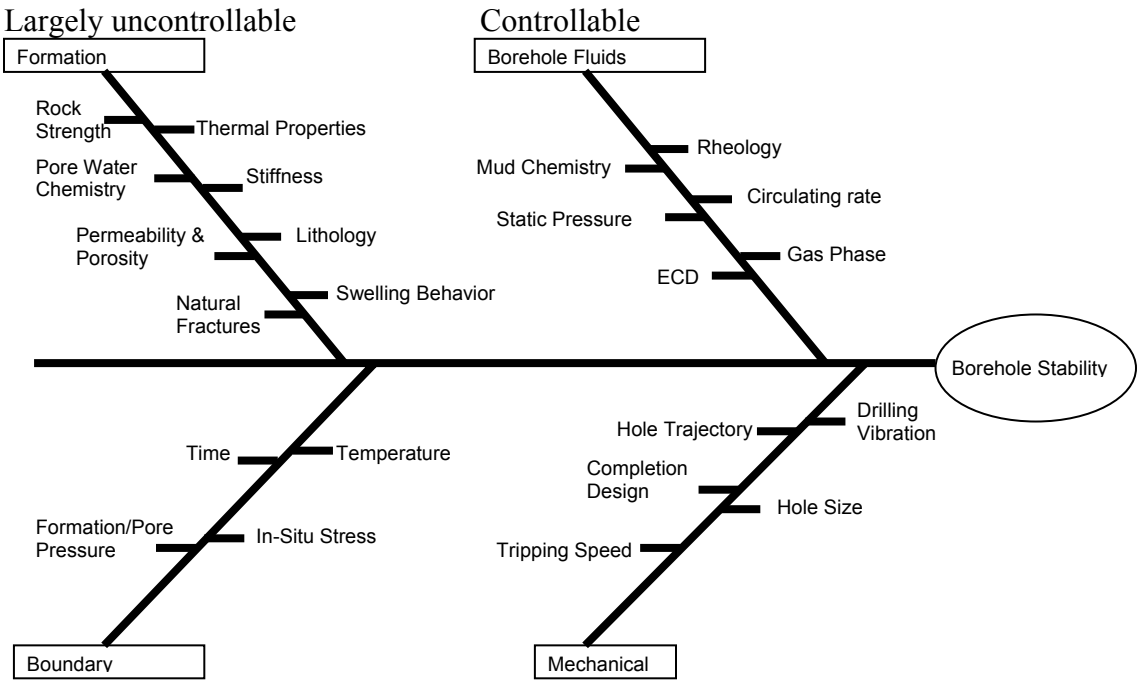

Fig. 5.1− Factors affecting wellbore stability[16]

5.2 Wellbore Stability in Shale

Shale makes up over 75% of drilled formations and causes over 90% of wellbore instability problems.[17] Drilling of shale can result in a variety of problems ranging from washout to complete collapse of the hole. These problems are severe, costing the industry a conservative $ 500 million/year problem.

Shale acts more like soil than rock, so predicting the correct behavior of shale is very dependent on its soil boring, water saturation, chemical aggregation, and particle size. That is why the density of shale changes from place to place. Shale can also act as an osmotic membrane. That means, in case of high water saturation, it can leak the water to the adjacent formation. For example, for water-based mud, the adjacent shale to the borehole can release its water through the mud and reduce the pore pressure in the immediate vicinity of the wellbore which results in wellbore instability. To model the shale, we have to incorporate the effect of stress induced by flow into or out of the formation, called poroelastic stress, and the chemical interaction between mud particles and the shale.

The model developed and used in this thesis is based on poroelasticity theory. The importance of this model is only for mechanical aspects of the shale to optimize borehole stability. Since in this thesis the well is cased, we assume no interaction between shale and drilling fluid. This study mostly deals with the interaction of shale and cement in the outer wellbore boundary.

5.3 Various Instability Risk Criteria

Various instability risk criteria will be shown:

- Shear yielding initiation at the wellbore wall.
- Cross-sectional area of rock yielding.
- Average radius of yielding zone.
- Total volume of yielded rock for a given stratigraphic unit.
- Total volume of yielded rock that detaches from the borehole wall.
- Borehole breakout width or angle.
- Rubble fill percentage for horizontal wells.
- Borehole wall convergence (squeezing in plastic shale).
- Hole enlargement from erosion.

5.4 Borehole Stability Analysis

Two models analyze borehole stability:

- Linear elastic behavior of the wellbore. In this model, the rock is assumed as a linear-elastic continuum. The calculations in this model are very simple but it never can model the effects of entering another zone after reaching the yield point. In other word; based on this model, the rock will fail if the stress continues to increase after yield point.
- Linear elasto-plastic behavior of the wellbore. In this approach, if the rock passes its peak of compressive strength, it will not necessarily fail completely. It may fail but not completely.

Models[18] based on linear elasticity do not adequately explain the fact that, in many cases, boreholes remain stable even if the stress concentration around the hole exceeds the strength of the formation. One option to compensate for this effect is to

implement a calibration factor. Alternatively, elastoplastic models offer the ability to assess the mechanical integrity of a borehole more realistically. These models recognize that even after a rock has been stressed beyond its peak strength, it does not necessarily fail completely and detach from the borehole wall.

CHAPTER VI
CEMENT BEHAVIOR ANALYSIS

In this chapter, we will summarize our assumptions described in the simulation software based on FEA. We have to fix the casing in some points in different situations to prevent casing movement because this analysis is mostly static; it leaves no space for casing to move. If it does move, the software will issue a warning that the system is unstable and can not tolerate this stress, and then it will crash.

Each simulation run requires certain assumptions. Different cements can tolerate different pressures and temperatures. In the case of HPHT wells, the use of proper cement is very important. In this work, we are not looking for physical properties of cement and its content. We are looking for the mechanical and thermal response of the cement in HPHT cases.

In this analysis, we model three different cases that we possibly can have on the wellbore:

- Wellbore with mud circulation.
- Wellbore without mud circulation during production.
- Wellbore under pressure testing.

6.1 Cement Behavior with Mud Circulation

Since mud circulates in the wellbore, the effect of formation temperature depends directly on the mud velocity and the time that mud stays in contact with the high-temperature formation. In our analysis, we account for thermal stress resulting from temperature difference by subtracting bottomhole static temperature from circulating bottomhole temperature. Laboratory studies show that stresses induced in the cement form the variation of downhole conditions that cause cement failure. [19-21]

6.2 Cement Behavior Without Mud Circulation (During Production)

According to the principle rule of heat transfer, the temperature will change in a system with two different temperatures until they reach equilibrium. These changes may be completed in an infinite time, but they are still important in short time periods.

Increasing pressure and temperature during production mainly concerns the near-surface casing sections, where surface pressure is increased from near atmospheric pressure to production pressure, and the temperature is increased to near-downhole temperature. The pressure variation usually concerns only the production tubing and does not affect the cemented sections, unless a gas migration problem results in an annulus pressure increase. A temperature increase also can lead to pressure increase or decrease in the annulus following gas expansion, if the annulus is saturated with gas. In the real-gas behavior formula, disregarding *z-factor*, pressure changes directly with temperature and inversely with volume.

6.3 Wellbore Under Steamflood in Different Temperatures

When enhanced oil recovery procedures were introduced to the industry, thermal stresses in and around the wellbore were discovered and after that the effect of coupling the thermal and mechanical stresses came to the investigation to better forecast the behavior of casing and cement during different thermal pilots.

6.4 Modeling

In this project, the stresses in the cement are calculated assuming that steel, cement, and rock are thermo-elastic materials and that the steel/cement interface and the cement/rock interface are either fully bounded or unbounded. Finally, the analysis presented here, assumes that the cement is under no internal stress after setting; only the variations of pressure, stress, or temperature that occur once the cement is set are considered.

The geometry of the problem is axisymmetric with the axis of symmetry being the wellbore axes, allowing the use of cylindrical coordinates r, θ, and z. The simplest situation is when the boundary and initial conditions (wellbore pressure, far-field state of stress, wellbore, and far-field temperature) are independent of θ. The variables of interest are then the radial displacement, radial stress, σ_r; tangential stress, σ_t; axial stress, σ_x; the shear stress τ, and temperature, T.

We model the wellbore with casing, cement, and the formation in one play. (*Play*, means the acting system of casing, cement, and formation.) This play can be very big or small in diameter or thickness. The hydrostatic mud pressure from the wellbore is the inner pressure in this play, and the horizontal in-situ stress acting on the outer boundary of cement is the outer pressure.

In this literature, we calculate all the rock mechanics parameters in Cartesian coordinate. There is no unit conversion in this literature regarding to this matter. The conversion has been done before the putting data sets in the FE simulator.

We ran some limited models just to investigate the effect of solid rock mechanics such as Young's modulus, Poison's ratio, and the effects of temperature, eccentricity, pressure differential and casing or cement thickness.

In these literatures[22-24]different types of cement were studied and applied to different wells. **Table 6.1** to **Table 6.4** governs the required data. Based on the type of additives and wellbore pressure and temperature, the solid mechanics behavior of the set cement changed and some of the cements failed in either internally or from boundaries. In this study, we are using the same cement characteristics in our modeling to monitor the behavior of these cements in various pressure and temperature conditions.

Table 6.1− Mechanical and Thermal Properties of Different Constituents [22-24]

(M=1000)

	Young's Modulus MMPSI	Young's Modulus 10^9 Pa	Poisson's Ratio ν	Specific Heat Btu/Lb. ^oF	Thermal Conductivity Btu/hr. ft. ^oF	Thermal Expansion Coefficient F^{-1}
Steel	29	199.9	0.27	0.11942	8.667	13E-6
Rock	1.45	9.997	0.2	0.2388	0.5778	1E-5
Cement	0.725	0.4998	0.2	0.5016	0.5778	1E-5
Slurry-1	1.2	8.274	0.1			
Slurry-2	0.174	0.12	0.17			
Slurry-3	0.566	0.39	0.15			
Slurry-4	0.571	0.394	0.23			
Slurry-5	0.015	0.0103	0.12			
Slurry-6	0.49	0.3379	0.21			
Slurry-7	0.44	0.3034	0.18			
Slurry-8	0.43	0.2965	0.19			
Slurry-9	0.95	0.655	0.18			
Slurry-10	0.74	0.51	0.24			
Slurry-11	0.66	0.455	0.22			
Slurry-12	1.45	9.998	0.15			
Slurry-13	0.094	0.0648	0.2			
Slurry-14	0.145	0.1	0.2			
Slurry-15	0.094	0.0648	0.2			
Slurry-16	0.145	0.1	0.2			
Slurry-17	0.145	0.1	0.2			
Slurry-18	0.45	0.31	0.2			

Table 6.2− Cement Property Definition

Cement Type	Property Description
Slurry-1	Class G [22]
Slurry-2	Hybrid [22]
Slurry-3	Latex-Slurry [22]
Slurry-4	Foamed Slurry-I [22]
Slurry-5	Foamed Slurry-II [22]
Slurry-6	Class A with 15%Multi Purpose Additive, .4%Extender Sodium Silicate, 0.45% CMHEC, .25% SNSC [23]
Slurry-7	Class A with 0.36gr Extender Sodium Silicate, 0.45% CMHEC [23]
Slurry-8	Class A with 6%Extender Bentonite [23]
Slurry-9	Class A with 0.2% CMHEC, 0.2% SNSC [23]
Slurry-10	Class A with 50%Multi Purpose Additive, 0.15% CMHEC, 0.15% SNSC [23]
Slurry-11	Class A with 15%Multi Purpose Additive, 0.25%Extender Sodium Silicate, 0.8% CMHEC, 0.45% SNSC [23]
Slurry-12	Conventional neat Cement [24]
Slurry-13	Flexible Cement [24]
Slurry-14	Flexible Cement (different from Slurry-13) [24]
Slurry-15	Flexible and Expanding(based on Slurry-13) [24]
Slurry-16	Flexible and Expanding (based on Slurry-13more expandable than Slurry-15) [24]
Slurry-17	Flexible and Expanding (based on Slurry-13more expandable than Slurry-16) [24]
Slurry-18	Atmospheric foamed cement (30% quality) with expanding agent [24]

Table 6.3− Geometry, Formation, and Fluids Data at Intermediate Casing[23]

Geometry Information		Formation and fluid Information	
Hole Size, inch.	12.25	Mud Density, ppg	14.5
Casing OD, inch.	9.875	Cement, ppg	15.5
Casing ID, inch.	8.539	Displacement Fluid, ppg (Casing)	14.5
		Displacement Fluid, ppg (Production Liner)	17.1
Casing Grade	Q125, 67.5 lb/ft	Completion Fluid, ppg	8.4
Depth (TVD), ft	16000	Formation Type	limestone
Previous Shoe (TVD), ft	12000	Formation Vertical Stress Gradient, psi/ft	0.94
Eccentricity, %	10	Formation Pore Pressure, psi/ft	0.46
		Formation Fracture Pressure, psi/ft	0.62

Table 6.4− Pressure/Temperature in Intermediate Casing During Well Events[23]

Event	Remarks	T_s' °F	$T_s' - T_c'$ °F	BHP- Pp psi	BHP- P_f psi
Completion	Displacement fluid inside the casing	350	50	12064-9280	12064-9920
	Completion fluid inside the casing	350	60	6989-9280	6989-9920
Pressure Testing	Completion fluid inside the casing	350	60	6989-9280	6989-9920
Hydrocarbon Production	Production Through Liner	350	0	15392-9280	14227-9920

The most reliable equation for calculating fracture pressure in the gulf coast is Ben Eaton's equation and can be written as Eq. 6.1.

$$\sigma_H = (\frac{\nu}{1-\nu})(\sigma_{ob} - p_p) + p_p, \quad \text{(6.1)}$$

The fracture gradient depends upon the location, depth, and formation. (In off-shore wells, the quantity of fracture gradient varies with the depth of water)

For depth of 16000 ft at the gulf coast margin in Texas, Poisson's ratio is equal to 0.25 in the calculations on **Table 6.4**.

Eq. 6.1 explains the upper limit of the inside wellbore pressure. If the pressure inside the wellbore exceeds this amount, it means that we pass the fracture pressure and we are fracturing our system ourselves, which is not desirable. As a consequence, we are endangering the whole structure to gas migration phenomena, and following that, the structure will collapse.

CHAPTER VII

RESULTS

Results that had an extreme effect on the case study reveal the effects of Young's modulus, Poisson's ratio, casing thickness, cement thickness, casing eccentricity, and temperature effect on each case.

Fig. 7.1 shows the model that we made. Notations on the figure are described as follows:

Area A, the system is under constraint load to lateral sides which means that the system can not move axially on the y-axis but it is free to move on the x-axis. Area B shows the type of analysis, which is nodal, and some governing data regarding the type of solution, like central processor unit, CPU, time. Area C is an index to the colors used in the analysis. These color codes are based on the intensity of the stress in each region. The number beside each color shows the magnitude of the stress at the area. The units in each figure are consistent with the input data units.

The correct behavior of the system can be found in the areas above or below the constraint-acting area. Since Young's modulus is the ratio of stress to strain, this number is a good basis for the flexibility of each medium or solid. If this parameter is too low, the medium will act plastically, like unconsolidated sand stone with high water saturation, and result in system instability. But if this number is low, the range of stresses which can be handled by the system will increase. The higher the Young's modulus, the stiffer the mass is. As it is shown in Fig. 7.1 (applying input data from **Table 7.1**) when the Young's modulus of cement is very high, in this case 10 times more than Young's modulus of casing, almost all the force is being applied to the casing, all deformation will be in the casing, and the cement will remain intact. In this situation, because the cement is acting more flexible than casing, it may cause casing to move and consequently increase the friction of the drill string in the wellbore resulting to early corrosion. As Fig. 7.1 shows, the strain in the casing is 20 times more than cement. It means that the casing failure is more possible than cement failure and as a result of casing failure, we have casing/cement boundary fail or de-bonding.

The effect of Poisson's ratio is significant. Since Poisson's ratio is the ratio of transverse contraction strain to longitudinal extension strain in the direction of the applied

force. In this study, since the model is investigating in 2D form, Poisson's ratio plays an extreme role in mass deformation. The plane-strain assumption based on no displacement along the wellbore direction is recommended for field use, so increasing transversal strain should increase in Poisson's ratio or vice versa.

TABLE 7.1− Input Data Required for Different Cases

Case	High cement Young's modulus	Low cement Poisson's ratio	High cement Poisson's ratio	High pressure difference	Thermal stress	Casing eccentricity	Casing/cement thickness
Event	completion	completion	completion	pressure test	completion	completion	completion
Slurry type	1	1	1	1	1	1	1
Casing ID	3	3	3	3	3	3	2
Casing OD	4	4	4	4	4	4	3.5
Casing Young's modulus	30 e 6	31 e 6	32 e 6	33 e 6	34 e 6	35 e 6	36 e 6
Casing Poisson's ratio	0.27	0.27	0.27	0.27	0.27	0.27	0.27
Cement OD	6	6	6	6			4
Cement Young's modulus	300 e 6	4 e 6	4 e 6	300 e 6	4 e 6	4 e 6	0.74 e 6
Cement Poisson's ratio	0.22	0.01	0.4	0.22	0.2	0.2	0.24
Bottomhole pressure	9280	9280	9280	10000	9280	9280	12064
Pore pressure	12064	12064	12064	15000	12064	12064	9280
Temperature	350	350	350	350	400	350	350

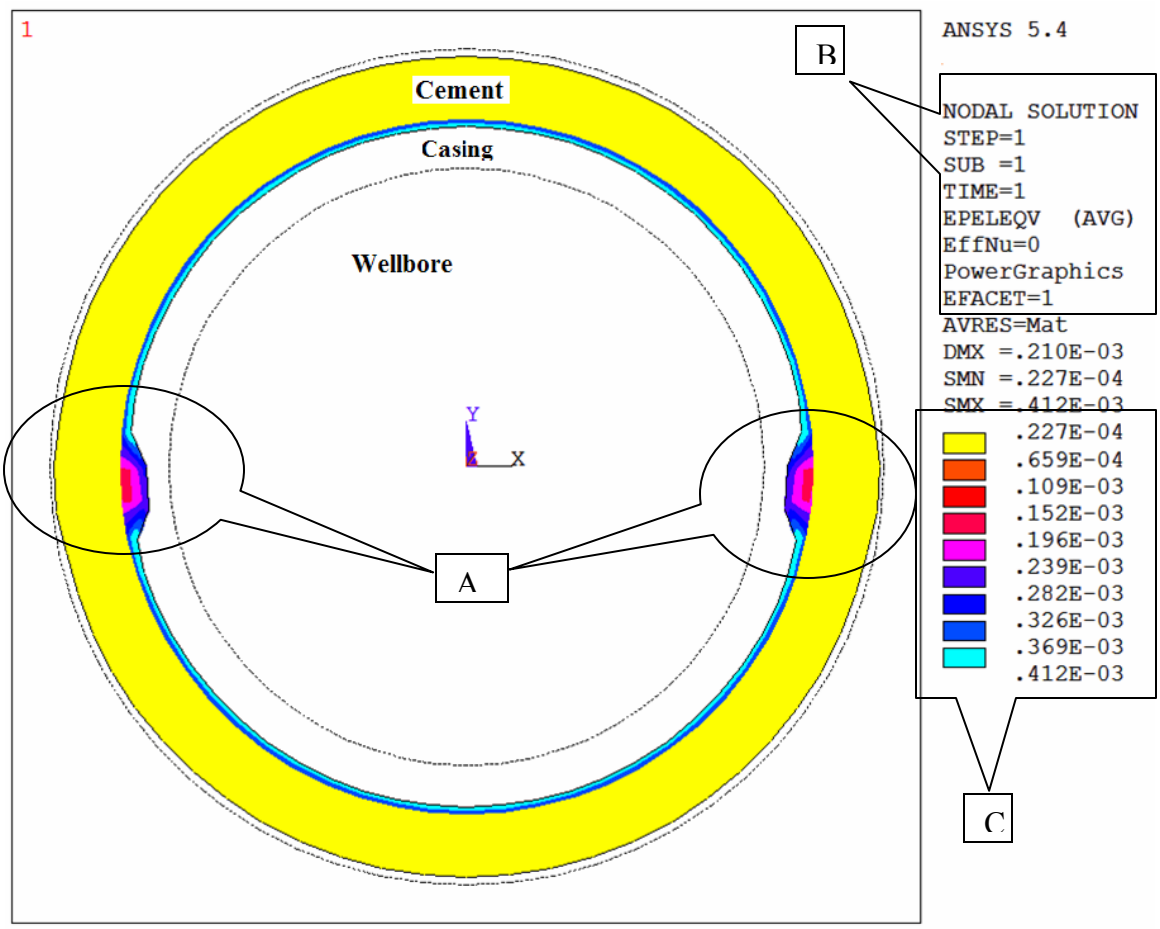

Fig. 7.1− Strain deformation while changing Young's modulus of cement ($E_{cement}=10\times E_{casing}$)

Fig. 7.2 (applying input data from **Table 7.1**) will resolve this effect more sensibly. In these cases, since the steel Poisson's Ratio is hard to change with respect to cement, including additives in the cement will keep this parameter in a reasonable range in any type of well completion.

If the two runs on Fig 7.2 and **Fig 7.3** (applying input data from **Table 7.1**) are compared with each other, the result is interesting. The cement had some deformation, laterally and radially, because of the difference between its Young's modulus and the formation. The effect of Poisson's ratio as shown is not significant. (The major deformation is because the low Young's modulus does not change Poisson's ratio but the range of Poisson's ratio has been changed by a factor of 40 in these two figures.)

The effect of pressure is very important in underbalanced drilling. The effect of pressure difference between the inside and outer boundary will change the results significantly and may cause expensive damage and permanent deformation in the system. **Fig. 7.4** (applying input data from **Table 7.1**) shows the effect of a 5000-psi difference between the inner and outer boundary conditions of the system. This case runs under the same conditions as earlier ones. To ignore the effect of probable inside casing damage, we assume that the entire casing is fixed and the pressure difference causes no expansion or contraction on casing. Because both Young's modulus and Poisson's ratio are very pressure dependent, the behavior of pressure in such system should follow the same as Young's modulus and Poisson's ratio. Referring to Poisson's ratio by definition, we can conclude that the strain distribution in case of having differential pressure on the system should follow exactly the same behavior as Poisson's ratio. This can be proved comparing Fig. 7.2, and Fig. 7.4.

Temperature has a huge effect on the system. Since the solid mechanic properties of the combined masses are strongly interconnected with temperature, its variation will cause some failure in the material composition and increase corrosion in the presence of corrosive fluids. The effect of temperature has been denoted in **Fig. 7.5** (applying input data from **Table 7.1**). In this figure, the Area D cement-casing edge has been put under another 50^0F thermal stress. Obviously, this imposed temperature increases the chance of failure in that section.

Eccentricity has its own case study. Based on type of cement, casing, inner and outer pressures, and enforced temperature, this parameter becomes important. **Fig. 7.6** (applying input data from **Table 7.1**) denotes the relative behavior of eccentricity of the casing. If we couple the effect of thermal stress and eccentricity, we come up to a severe scenario for cement failure. In this situation, the chance of cement/casing Debonding will be the same all over the boundary regardless of cement thickness.

Casing thickness and cement thickness have been investigated in **Fig. 7.7**. The relevant data for this run are located in **Table 7.1**. In this case where the ratio of casing thickness to cement thickness is more than 2, the dominant stress concentration will be focused on the layer with higher the Young's modulus, because the more flexible matter will transmit the stress or strain to the adjacent matter. In such cases, there may be some de-

bonding may appear in the margin between two different materials as a result of corrosion in the long-term wellbore life, especially in HPHT cases.

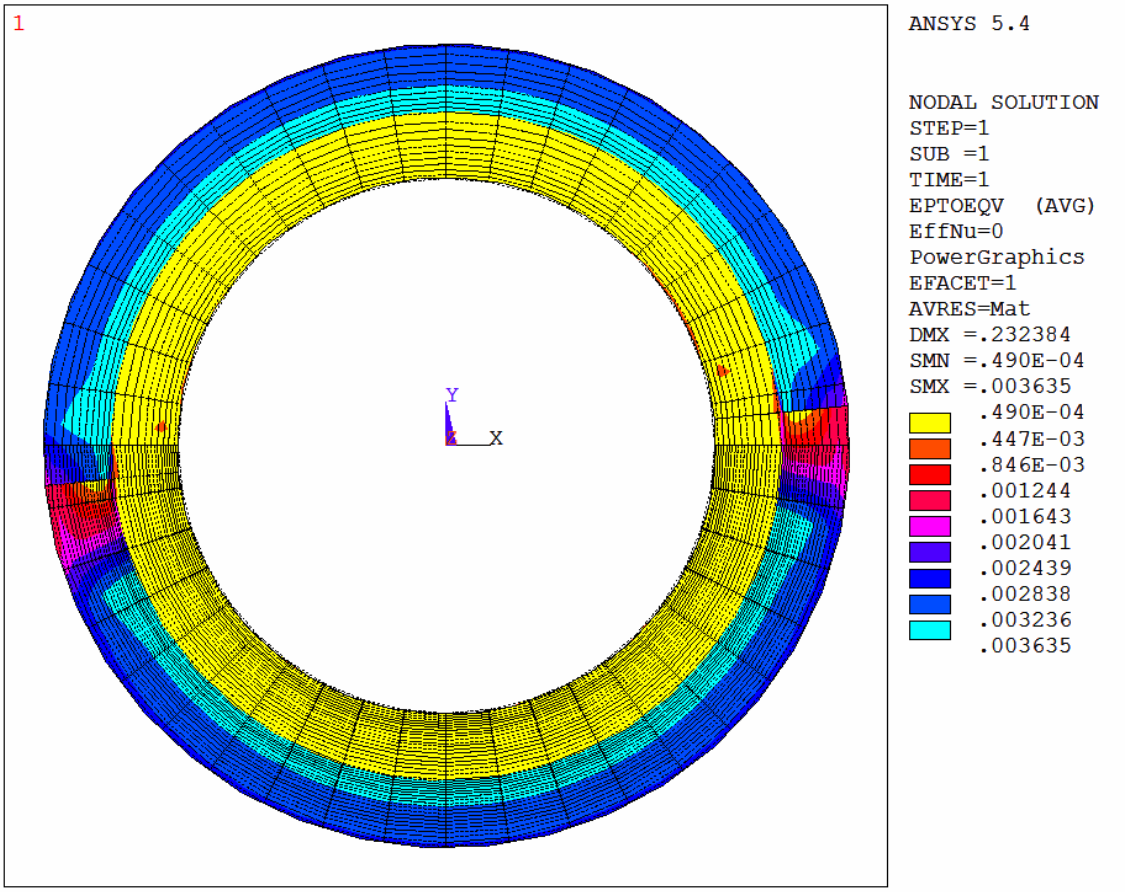

Fig. 7.2− Strain distribution while the Poisson's ratio is 0.01
(Strain is low in casing, very high in casing/cement boundary and lower in cement/formation boundary)

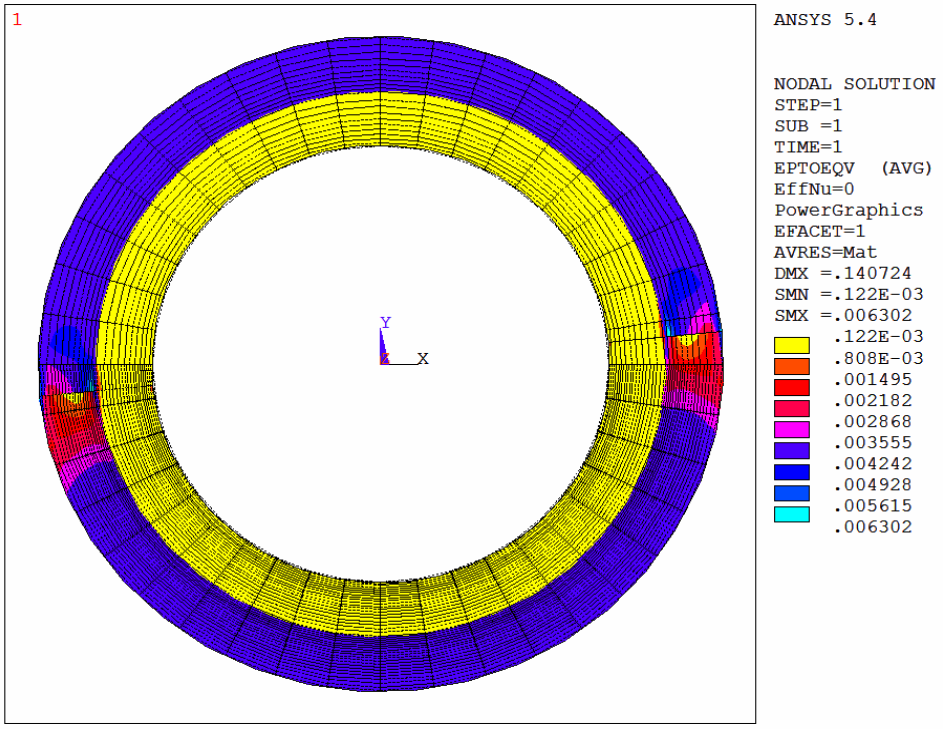

Fig. 7.3− Strain distribution while the Poisson's ratio is 0.4 (40 times more than Fig. 7.2. since quantity of Poisson's ratio of two adjacent matters is very close to each other, the strain distribution is uniform in each medium)

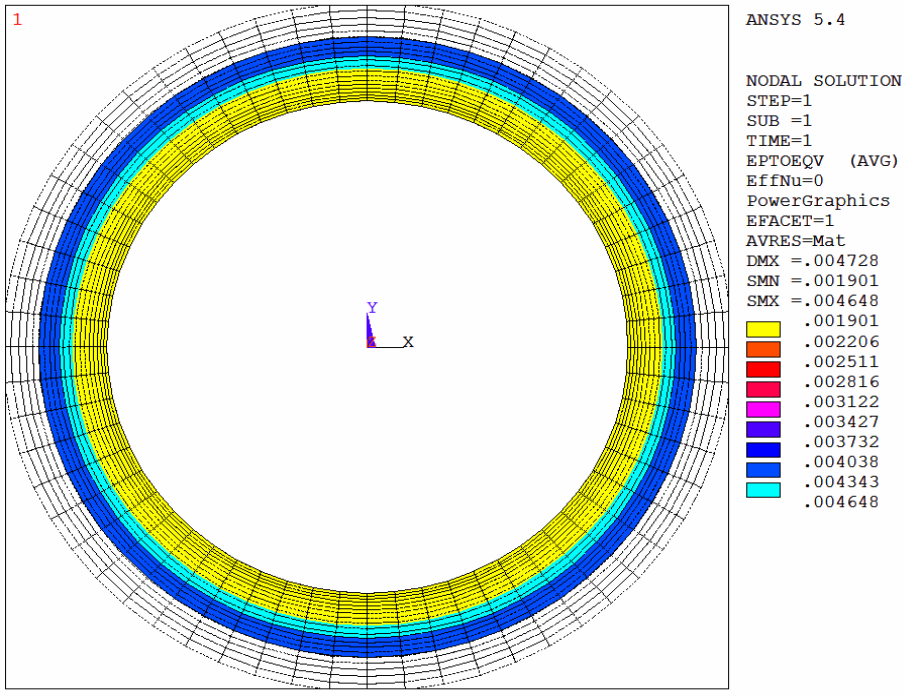

Fig. 7.4− Effect of high pressure difference between inside the casing and in the outer boundary of cement (in this case, the pressure difference is 5000 psi)

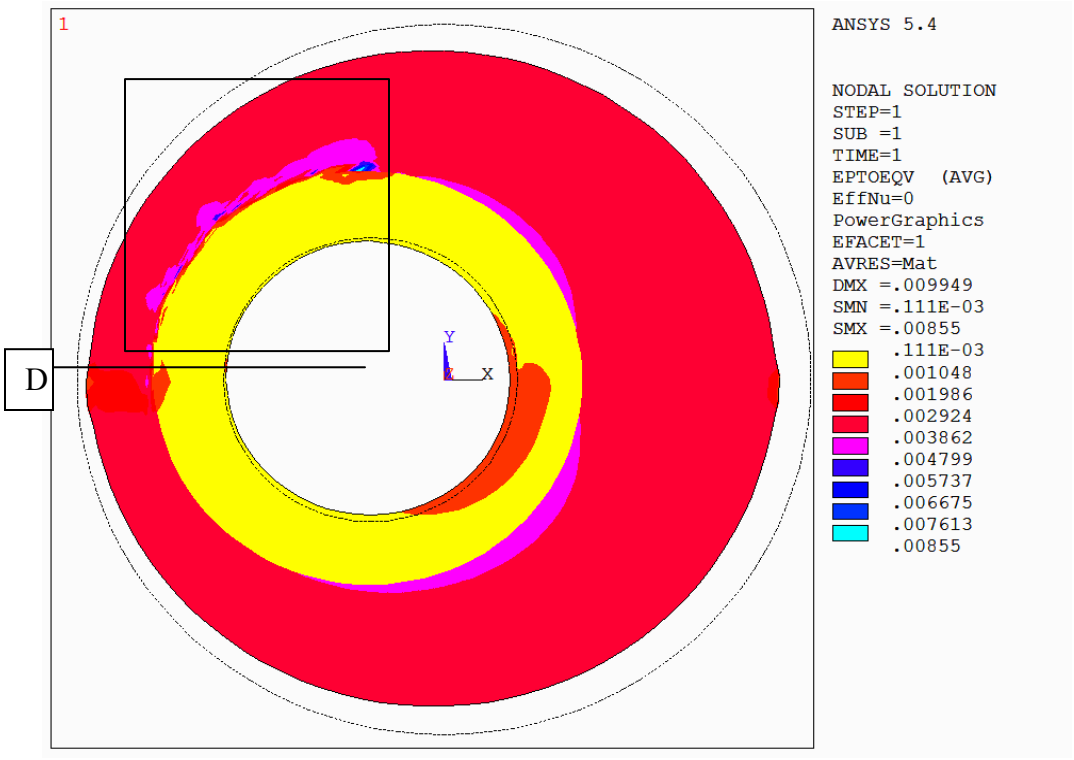

Fig. 7.5− Effect of temperature on the edge strain (extra temperature added on the cement-casing boundary in area D)

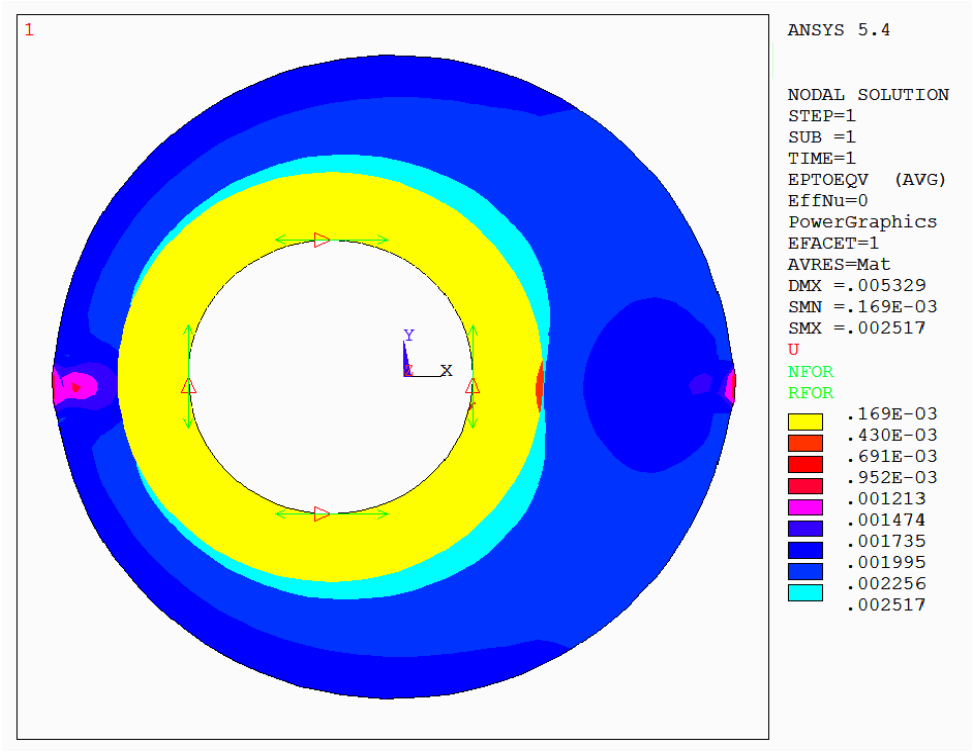

Fig. 7.6− Strain distribution in eccentric casing (Higher cement failure chance in thicker cement side)

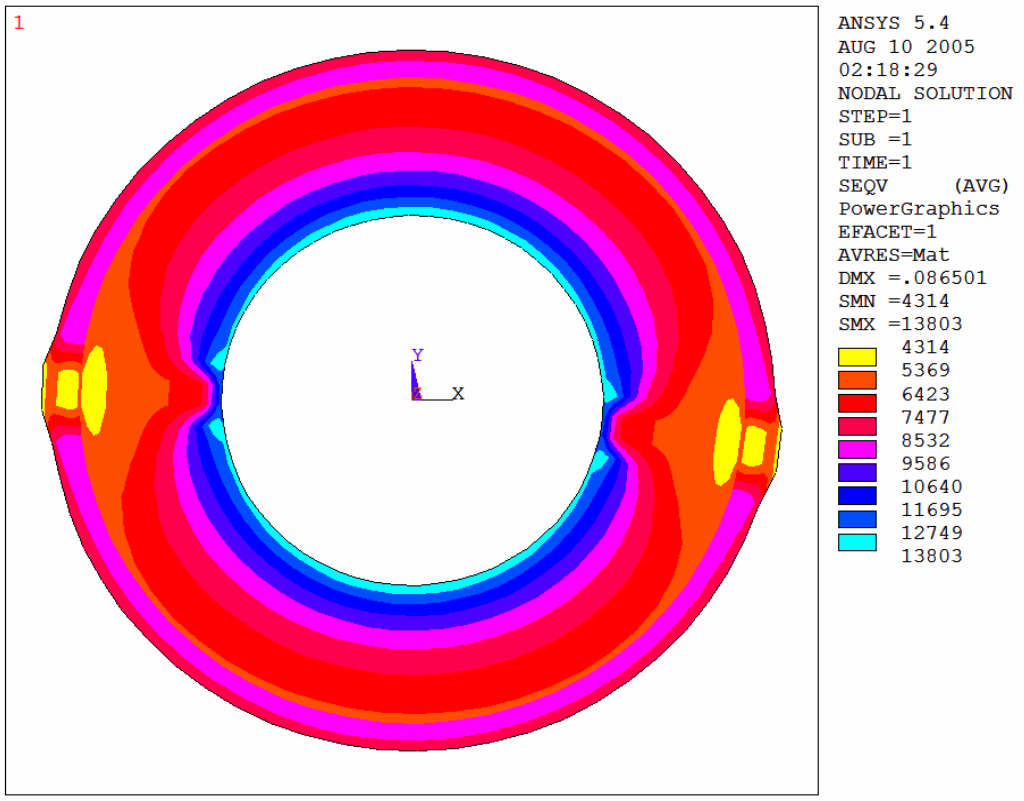

Fig. 7.7− Stress distribution while changing casing and cement thickness (The behavior is quite uniform and chance of failure is low)

In the **Fig. 7.8** the shear stress in X-Y coordinate has been sketched for the system covering data from **Table 7.2**.

Table 7.2− Input Data for Investigating Shear-Stress in Slurry-1

Event	Slurry Type	Casing ID, in	Casing OD, in	Casing Young's Modulus, psi	Casing Poisson's Ratio	Cement OD, in	Cement Young's Modulus, psi	Cement Poisson's Ratio	P_{BH}, psi	Pp, psi	Temperature, ^0F
completion	1	8.539	9.875	30e6	0.27	12.25	1.2e6	.1	6989	9280	350

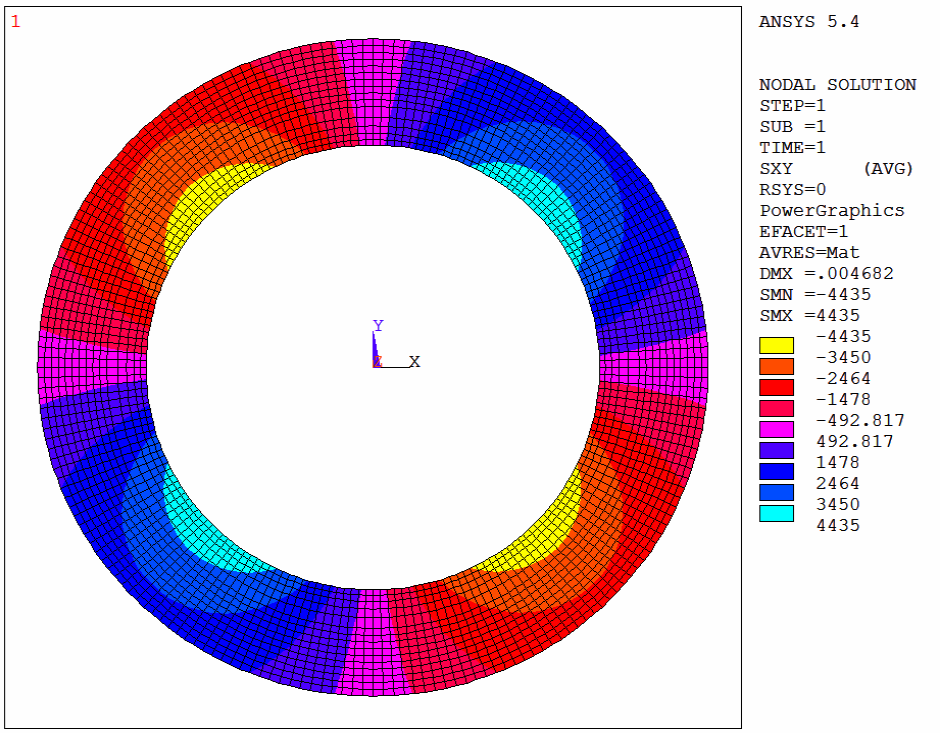

Fig. 7.8– Shear-stress distribution in x-y coordinates

In this scenario, four sections behave exactly the same but with the opposite sign of force as shown in Area C (Tension or compression).The primary assumed element (quadratic) is shown in **Fig. 7.9**. In this sketch, the sides of the element are exactly parallel and equal to each other.

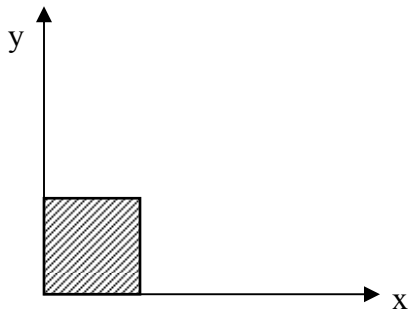

Fig. 7.9– Primary element model (quadratic, eight nodes)

The trend of shear stress in each quarter of the casing-cement system is maximized in the half. (*Half*; at 45^0 we encounter the maximum shear stress) But this shear stress

quantity is positive in the first and third quarters and negative but equal in the second and forth quarters. **Fig. 7.10** depicts the direction of maximum shear and the reflection of primary element to that in the first quarter. Those elements on the second and fourth quarter behave as shown in **Fig. 7.11**.

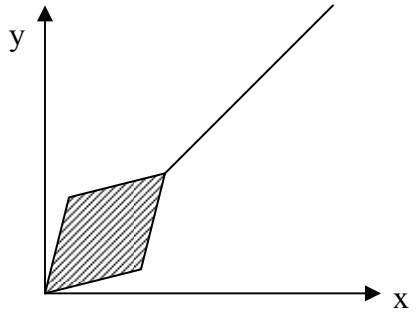

Fig. 7.10− Element verification in 1st and 3rd quarters

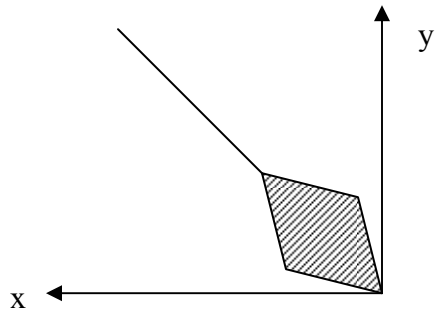

Fig. 7.11− Element verification in 2nd and 4th quarters

To investigate the cement or casing behavior, we need to know the shear stress of each. According to Fig 7.8 if the cement passes the limit of maximum shear, it will fail.

The rock properties of cement will change depending on the its make up. In this simulation, since the meshes are not too fine, the final shear stress behavior of all the slurries (tabulated in **Table 6.1)** in one set of inside and outside pressures will be the same. But since the shear stress is strongly related to cement aggregation, the pressure won't be the same, and some slurries will fail. (Slurries in set cement form)

If we force another set of pressures inside and outside the system, **Fig. 7.12** (sketch based on **Table 7.3** data) the reaction of the entire system will change with new applied pressures. Cement behavior under this circumstance is strongly related to its aggregation and the induced pressures.

Table 7.3− Input Data for Shear-Stress Test on Slurry-9

Event	Slurry Type	Casing ID, in	Casing OD, in	Casing Young's Modulus, psi	Casing Poisson's Ratio	Cement OD, in	Cement Young's Modulus, psi	Cement Poisson's Ratio	P_{BH}, psi	Pp, psi	Temperature, ^{0}F
completion	9	8.5 39	9.8 75	30e6	0.27	12.2 5	.95e6	.18	9280	15392	350

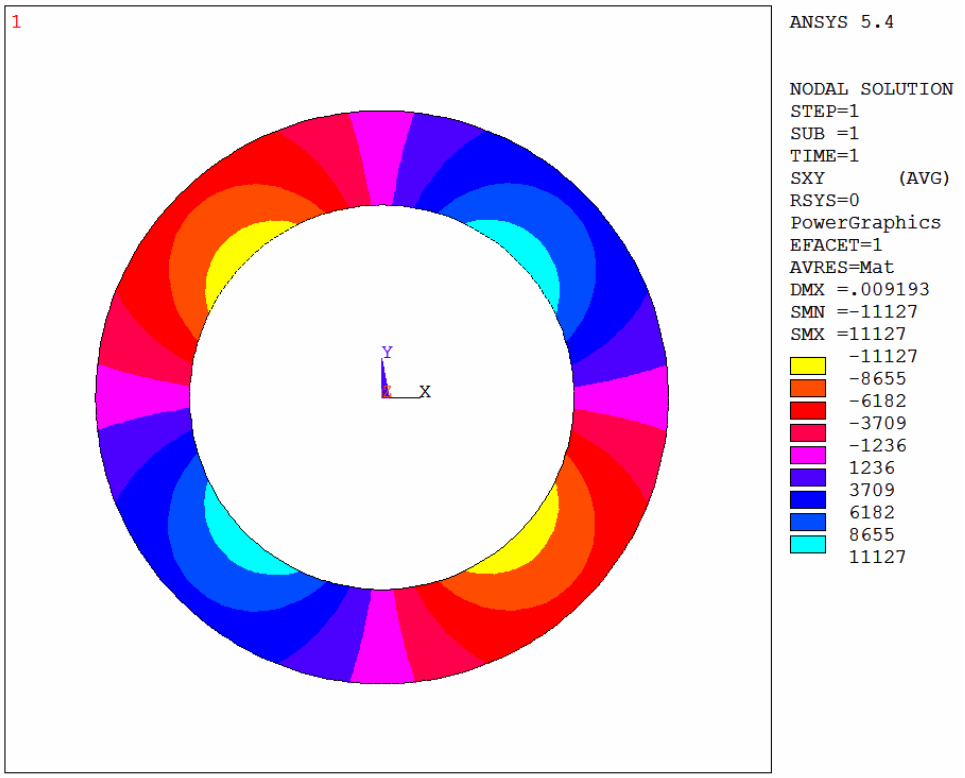

Fig. 7.12− Shear-stress profile in case of forcing higher outside pressure

Because the same cement is under different imposed pressure in the same well, the chance of failure increases. The failures are mostly cement-casing parting, cement-formation parting, and cement breakage.

According to Eq. 7.1 shear-stress changes with area (A) and thickness, moment of inertia of the passive surface and shear force (F). In this case, the area and thicknesses remain constant, so shear-stress is just changing under applied force (F), which is why whenever the force goes up, the shear stress increases linearly.

$$\tau = \lim_{\Delta A \to 0} \frac{\Delta F}{\Delta A} \quad \text{..... (7.1)}$$

The acting force and cross-sectional area are shown in **Fig. 7.13**.

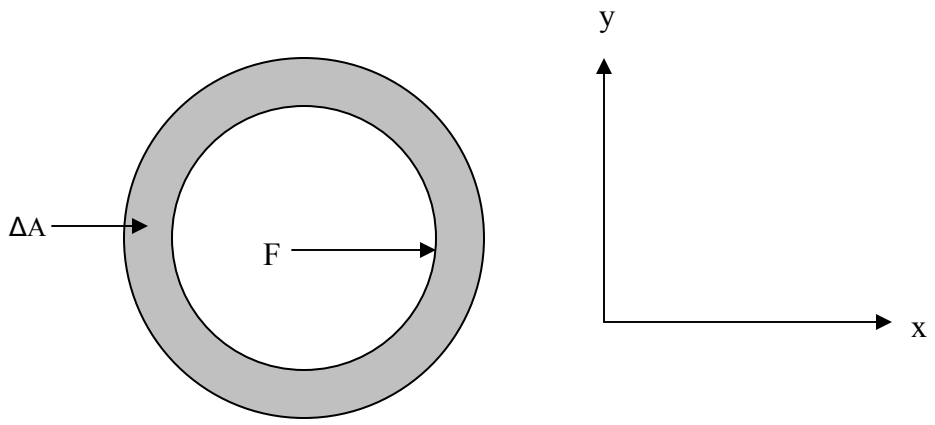

Fig. 7.13− Active force and the cross sectional area

The deformation caused by shear-stress is called *shear-strain*. The ratio of shear-stress to shear-strain based on Hook's law is called shear module of elasticity; G. Shear-strain is depicted in **Fig. 7.14**.

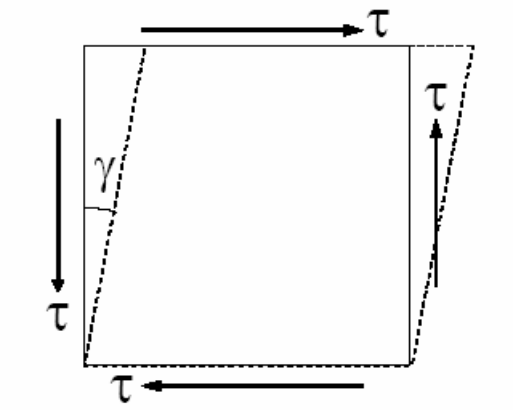

Fig. 7.14− Element of material with applied shear-stress, τ , and shear-strain, γ

The behavior of shear-stress is dependent on the amount of pressure acting on the system. Since no shear-stress data are available for the cements that have already been modeled, we cannot conclude any form of deformation for those systems. But since the cement is very shear dependent and will collapse under high shear-stress, we can infer that the system may fail if it goes under frequent pressure testing.

The following cases illustrate casing-cement interaction with different cement solid properties under different sets of imposed pressures. **Table 7.4** governs data needed for **Fig. 7.15.** If we compare the results in **Fig. 7.15** and **Fig. 7.16** (ignoring the change in Young's modulus and Poisson's ratio, **Table 7.5**), we can conclude that both shear-stress and shear-strain are related to pressure changes rather than changes in cement properties. It does not mean that shear-stress or shear-strain are independent from the material properties of solids, but it means that these parameters (shear-stress and shear-strain) mostly take the advantage of pressure variations.

Table 7.4− Input Data for Investigating Shear-Strain in Slurry-2

Event	Slurry Type	Casing ID, in	Casing OD, in	Casing Young's Modulus, psi	Casing Poisson's Ratio	Cement OD, in	Cement Young's Modulus, psi	Cement Poisson's Ratio	P_{BH}, psi	Pp, psi	Temperature, ^0_F
Pressure Testing	2	8.539	9.875	30e6	0.27	12.25	.174e6	.17	9280	15392	350

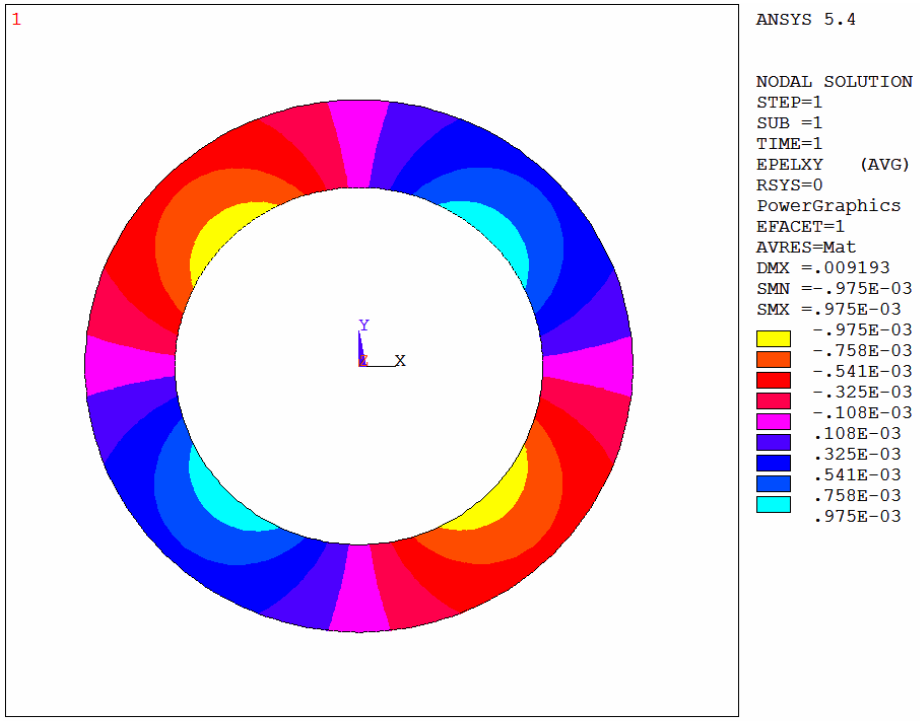

Fig. 7.15− Shear-strain test in pressure test (high pressure)

Table 7.5− Input Data for Investigating Shear-Strain in Slurry-4

Event	Slurry Type	Casing ID, in	Casing OD, in	Casing Young's Modulus, psi	Casing Poisson's Ratio	Cement OD, in	Cement Young's Modulus, psi	Cement Poisson's Ratio	P_{BH}, psi	Pp, psi	Temperature, ^0_F
Pressure Testing	4	8.539	9.875	30e6	0.27	12.25	.571e6	.23	6989	9280	350

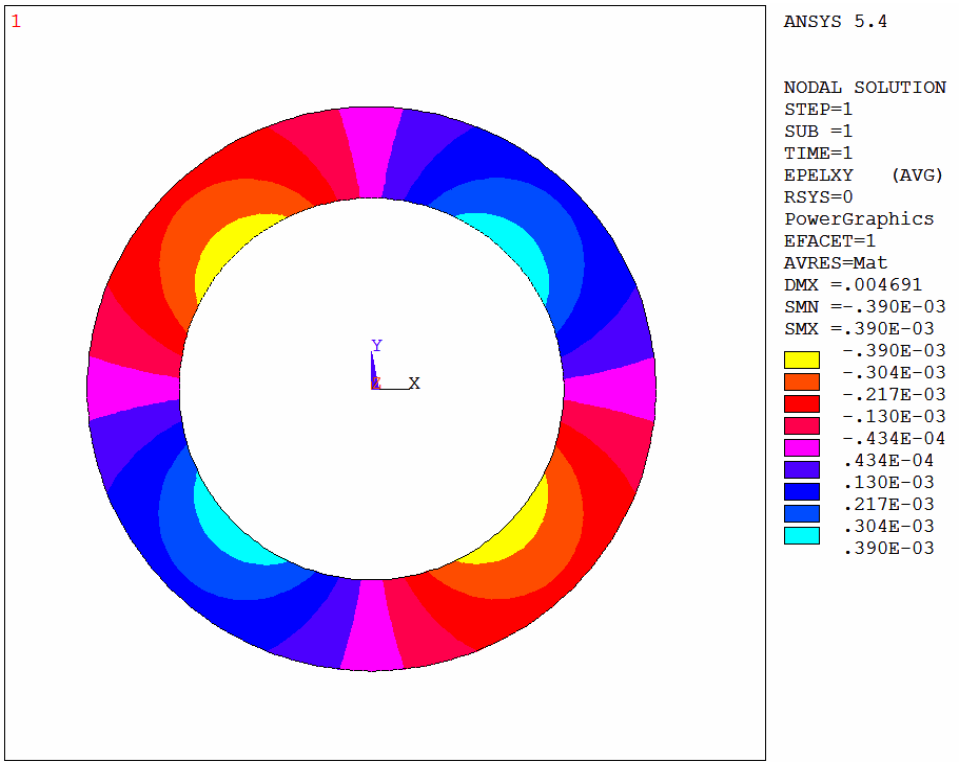

Fig. 7.16− Shear-strain test in pressure test (low pressure)

The von-Mises failure criterion is known as the average resultant stress criterion. Based on this application, whenever the two horizontal stresses are equal, this criterion react the same as other available criteria.(like Drucker-Prager) In **Fig. 7.17** the reaction of the system based on data labeled on **Table 7.6** under von-Mises criterion is depicted. Since everything is symmetric, the results are in symmetric form. As **Fig. 7.18** shows the minimum and maximum acting pressures are more than those we estimated.

Table 7.6− Input Data for Investigating Stress in Slurry-5

Event	Slurry Type	Casing ID, in	Casing OD, in	Casing Young's Modulus, psi	Casing Poisson's Ratio	Cement OD, in	Cement Young's Modulus, psi	Cement Poisson's Ratio	P_{BH}, psi	Pp, psi	Temperature, ^0_F
Pressure Testing	5	8.539	9.875	30e6	0.27	12.25	.015e6	.12	6989	9280	350

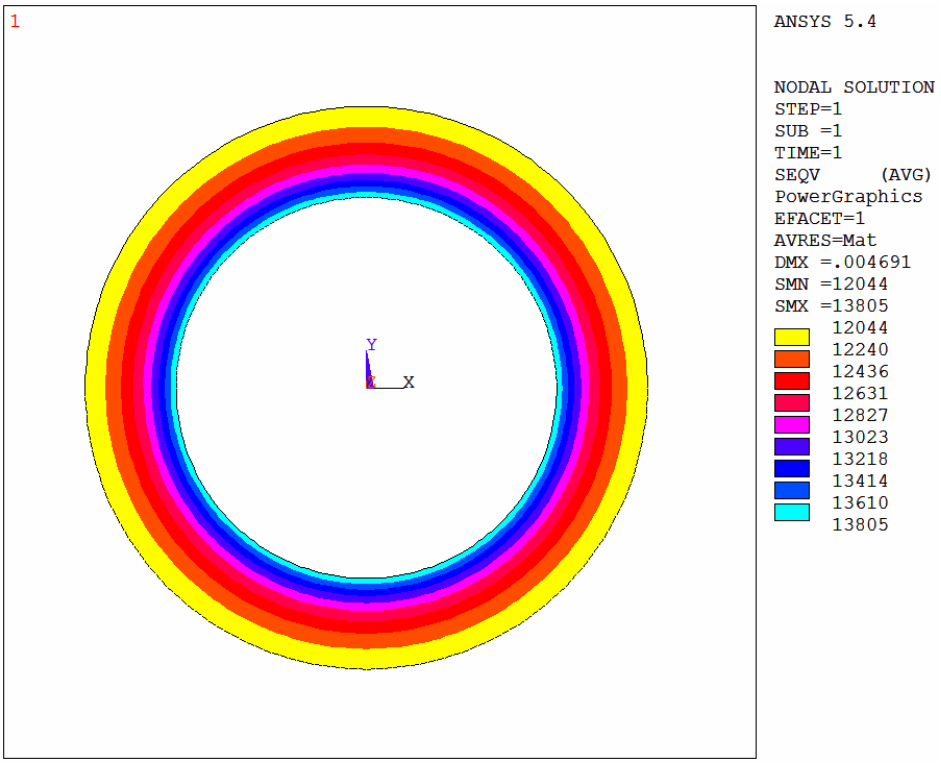

Fig. 7.17− Stress profile based on von-Mises criterion in pressure test

Fig. 7.18 and **Fig. 7.19** (based on data in **Table 7.7**) show clearly the reaction of the system to higher inside pressure. Comparing Fig. 7.19 with Fig. 7.16 shows that if the dominant pressure forces changes (switch inside to outside), the system still reacts the same. This same reaction is mostly because of the material properties of the system attaching to each other. That is the reason we said that in previous runs that the shear-

stress and shear-strain are not just reacting because of induced pressure, but also because of the material properties of the system.

Table 7.7− Input Data for Investigating Shear-Stress in Slurry-13

Event	Slurry Type	Casing ID, in	Casing OD, in	Casing Young's Modulus, psi	Casing Poisson's Ratio	Cement OD, in	Cement Young's Modulus, psi	Cement Poisson's Ratio	P_{BH}, psi	Pp, psi	Temperature, ^0_F
Hydrocarbon Production	13	8.539	9.875	30e6	0.27	12.25	.094e6	.2	15392	9280	350

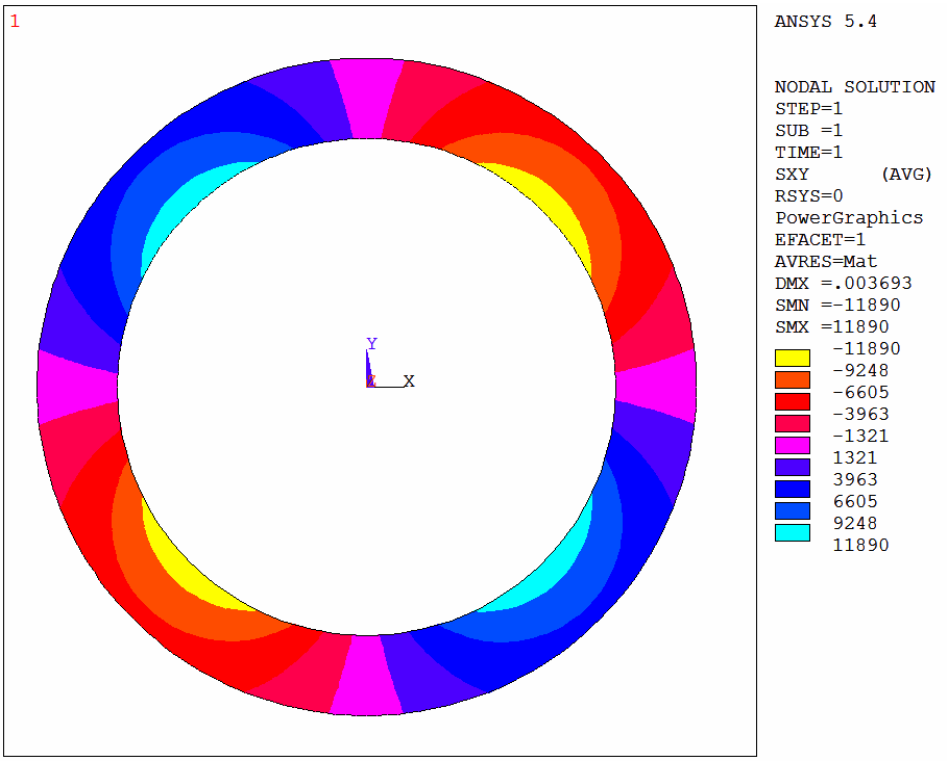

Fig 7.18− Shear-stress profile for slurry-13 under hydrocarbon production

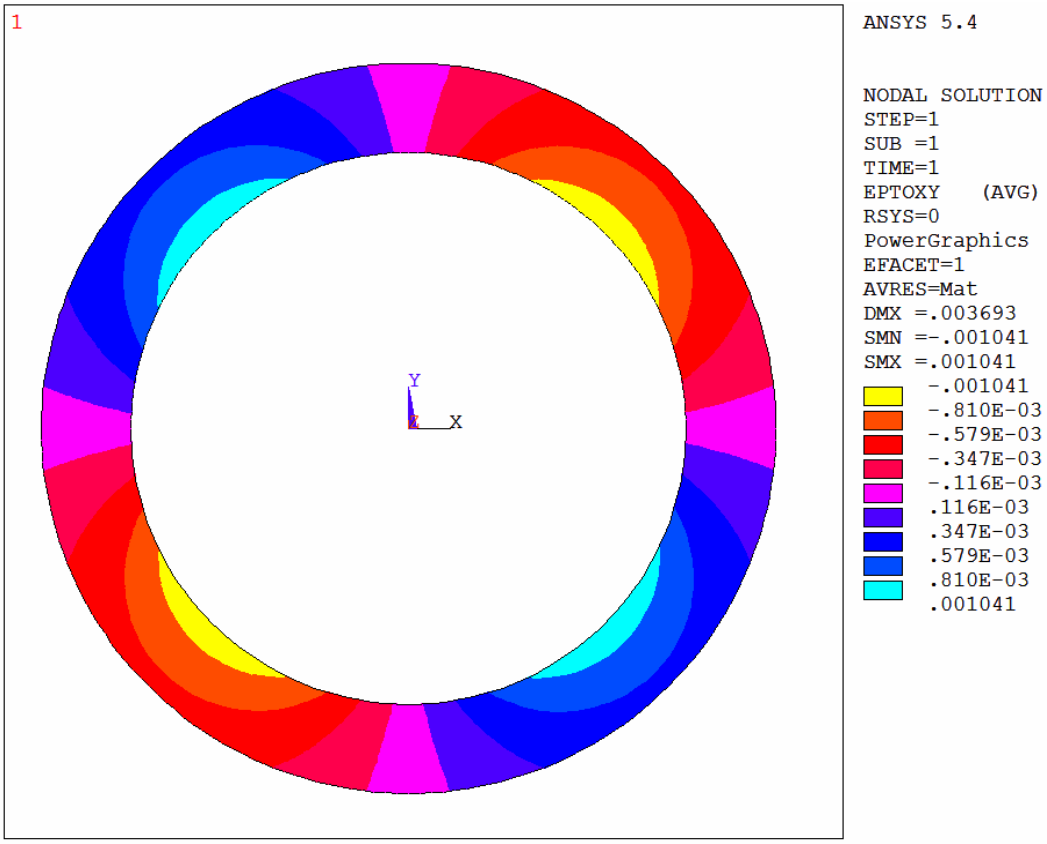

Fig 7.19– Shear-strain profile for slurry-13 under hydrocarbon production

CHAPTER VIII
CONCLUSIONS

This project has shown that:

1- Changing temperature can cause unexpected behavior in the cement sheath, which leads to failure in the casing/cement bond.

2- In the case of eccentric casing, the cement/casing bond will break radially, mostly on the side of the thicker cement sheath.

3- Early cement failure is likely to occur unless a low-shrinkage cement is used in HPHT wells.

4- Failure in the cement is strongly affected by wellbore temperature, formation temperature, cement thickness, casing diameter, and casing eccentricity.

5- Rock properties of the cement and casing such as Young's modulus and Poisson's ratio play extreme roles in this system. Increasing Young's moduli push the matter to the stiffer zone where it becomes more breakable under some pressure tests. Increasing Poisson's ratio leads the matter to act like plastic. So decreasing Young's modulus should be accompanied by increase in Poisson's ratio to keep the system intact over the loads of stresses coming under pressure testing.

CHAPTER IX

RECOMMENDATIONS

Some recommendations to consider for future work follow;

Investigate the effect of unequal horizontal stresses. This thesis has assumed that the quantity of $\sigma_{\min} = \sigma_{\max}$. Although this assumption is valid for Gulf of Mexico, it may not apply to other fields.

Try to investigate the effect of overburden stress through 3D modeling. This project has been limited to 2D modeling with constant amount of σ_{ob}.

Calculate the wellbore temperature via FDM. Temperatures in this project were merely based on published data.

Since shear stress is strongly dependent on forced pressure, designers should not ignore this important parameter. Merely lowering Young's modulus or raising Poisson's ratio may lead to poor cement design.

NOMENCLATURE

API	=	American Petroleum Institute
BHP	=	Bottom Hole Pressure
C	=	center of Mohr's circle
d_{ic}	=	Inside diameter of casing, ft (m)
d_{ot}	=	Outside diameter of tubing, ft (m)
E	=	Young's Modulus
k_h	=	Thermal conductivity, J/[m s K]
K_{hob}	=	Thermal conductivity of the adjacent media, Btu/hr-ft-^oF (KW/m-K)
K_{mk}	=	Matrix Stress Coefficient
m_f	=	Constant with dimensions of 1/Length
q	=	Heat loss rate in Btu/hr-ft-length (KW/m)
q_h	=	Heat flux, J/[m^2 s]
r	=	Radius of Mohr's Circle
S	=	Constant Which Depends on Rock Mass
s	=	Second
t	=	Time, hr
T^*	=	Absolute temperature, ^oR (^oK)
T_f	=	Formation temperature
T_S	=	Surface temperature
U	=	Heat Flow in Cement
α	=	Thermal conductivity of the media, ft^2/hr (m^2/s)
α_f	=	Volumetric coefficient of thermal expansion for the fluid
α_s	=	Volumetric coefficient of thermal expansion for the solid
Σ	=	View factor
ε_{ci}	=	Emissivity of the casing interior
ε_{to}	=	Emissivity of tubing exterior
*μ	=	Coefficient of Internal Friction

μ	=	Coefficient of Sliding Friction
σ_{ob}	=	Overburden Stress
σ_{t}	=	Tangential Stress
σ_{r}	=	Radial Stress
ν	=	Poison's Ratio
σ_{c}	=	Confining Stress
T_c'	=	Bottom Hole Circulating Temperature
P_F	=	Bottom Hole Fracture Pressure
P_f	=	Bottom Hole Formation Pressure
T_s'	=	Bottom Hole Static Temperature
dT / dZ	=	Thermal Gradient
σ_n	=	Normal Stress
σ_1	=	Maximum Horizontal Stress
σ_2	=	Minimum Horizontal Stress
τ	=	Shear Stress
T_s	=	Surface Temperature, F
T_c	=	Casing Temperature, F
σ'	=	Conversion Factor
ε'	=	Emissivity Coefficient
T_f	=	Formation Temperature, F
K_{hcem}	=	Cement Thermal Conductivity
K_{hs}	=	Surface Thermal Conductivity
d_{cem}	=	Cement external Diameter, in

REFERENCES

1 Casse, F. J.: "The Effect of Temperature and Confining Pressure on Fluid Using Pressure and Tracer Data," PhD dissertation, Stanford University., Stanford (1974).

2 Hudson, J. A. and Harrison, J. P.: *Engineering Rock Mechanics: An Introduction to Principles*, Elsevier, New York, NY 1997, 1-4.

3 North, J., Brangetto, M. P., and Gray, E.: "Central Garben Extreme Offshore High-Pressure/High-Temperature Cementing Case Study," paper SPE 59169 presented at the 2000 IADC/SPE Drilling Conference, New Orleans, LA, 23-25 February.

4 *RPI 10B Recommended Practice for Testing Well Cements*, 22nd edition, API, Washington, DC (1997)

5 Wooly, G. R., Giussani, A. R., Galate, J. W., and Wedelich III, H.F.: "Cementing Temperatures for Deep-Well Production Liners," paper SPE 13046 presented at the 1984 Annual Technical Conference and Exhibition, Houston, 16-19 September.

6 Martins, L., Campos, G., Silva, M. G. P., Miranda, C.R., and Teixeira, K. C.: "Tools for Predicting and Avoiding Gas Migration After Casing Cementing in Brazilian Fields," paper SPE 39008 presented at the 1997 Latin American and Caribbean Petroleum Engineering Conference and Exhibition, Rio de, Janeiro, Brazil, 30 August- 3 September.

7 Dean, G. D. and Brennen, M.A.: "A Unique Laboratory Gas Flow Model Reveals Insight to Predict Gas Migration in Cement," paper SPE 24049 presented at the 1992 Western Regional Meeting, Bakersfield, CA, 30 March-1 April.

8 Gallagher, R. H., Oden, J. T., Taylor, C., and Zienkiewicz, O. C. (Eds.): *Finite Elements in Fluids*, Vol. 1, John Wiley, New York (1975**)**.

9 Kaiser, M. J., and Mesyanzhinov D. V.: "Long-Term Oil and Gas Structure Installation and Removal Forecasting in the Gulf of Mexico: A Decision and Resource-Based Approach," *Oil & Gas J.* (May 2004) 46.

10 Bassiouni, Z.: *Theory, Measurement and Interpretation of Well Logs*, SPE Textbook Series, SPE, Richardson, TX (1994) **4**, 55-58.

11 Huygen, H. A. and Huitt, J. l.: "Wellbore Heat Losses and Casing Temperatures During Steam Injection," *Prod. Monthly* (Aug. 1966) 2-8.

12 Farouq Ali, S. M.: *Practical Heavy Oil Recovery*, HOR Heavy Oil Recovery Technologies Ltd, Oct. 2002, Chap.18, PP 7-11.

13 Eshelby, J. D.: "The Determination of the Elastic Field of an Ellipsoidal Inclusion, and Related Problems," *Proc. Roy. Soc*. A **241**, (1957), 376-396.

14 Labudovic, V.: "The Effect of Poisson's Ratio on Fracture Height," paper SPE 10307 presented at the 1981 SPE Offshore Europe Conference, Aberdeen, United Kingdom, 15-18 September.

15 Clifton, R.J. and Wang, J. J.: "Modeling of In-Situ Stress Change Due to Cold Fluid Injection," paper SPE 22107 presented at the 1991 International Arctic Technology Conference, Anchorage, AL, 29-31 May.

16 McLellan, P. and Hawkes, C.: "User-Friendly Borehole Stability Software for Designing Horizontal and Deviated Wells," paper presented at the 1999 CADE/CAODC Spring Drilling Conference, Calgary, AB 7-8 April.

17 Fonseca, C. F. H.: "Chemical-Mechanical Modeling of Wellbore Instability in Shale**s**," PhD dissertation, University of Texas at Austin (1997).

18 Goodwin, K. J. and Crook, R. J.: "Cement Sheath Stress Failure," *SPEDE* (December 1992) 291.

19 Jackson, P. B. and Murphey, C. E.: "Effect of Casing Pressure on Gas Flow Through a Sheath of Set Cement," paper SPE 25698 presented at the 1993 SPE/IADC Drilling Conference, Amsterdam, 23-25 February.

20 Bol, G. M., Wong, S. W., Davidson, C. J., Woodland, D. C.: "Borehole Stability in Shales," paper SPE presented at the 1997 European Petroleum Conference, Cannes, France, 16-18 November.

21 Thiercelin, M. J., Dargaud B., Baret J. F., and Rodriquez W.J.: "Cement Design Based on Cement Mechanical Response," paper SPE 52890 presented at the 1998 SPE Annual Technical Conference and Exhibition, San Antonio, TX, 3-5 October.

22 Bosma, M., Ravi, K., Driel, K., and Schreppers, G. L.: "Design Approach to Sealant Selection for the Life of the Well," paper SPE 56536 presented at the 1999 SPE Annual Technical Conference and Exhibition, Houston, TX, 3-6 October.

23 Di Lullo, G. and Rae, R.: "Cements for Long Term Isolation −Design Optimization by Computer Modeling and Prediction," paper SPE 62745 presented at the 2000

IADC/SPE Asia Pacific Drilling Technology, Kuala Lumpur, Malaysia, 11-13 September.

24 Boukhelifa, L., Moroni, N., James, S.G., Le Roy-Delage, S., Thiercelin, M.J. *et al*.: "Evaluation of Cement Systems for Oil- and Gas-Well Zonal Isolation in a Full-Scale Annular Geometry," *SPEDC* (March 2005) 44.

VITA

Name: Mehdi Abbaszadeh Shahri

Permanent Address: #72, West 220 St, Tehranpars Broadway
Tehran, 16868
Iran

Education:

B.S., Petroleum Engineering
Petroleum University of Technology
Ahwaz, Iran
(Sep. 1997 – Sep. 2001)

M.S., Petroleum Engineering
Texas A&M University
College Station, TX, 77843
USA.
(May. 2003 – Dec. 2005)